Am J Physiol Heart Circ Physiol 314: H627–H642, 2018.
First published November 22, 2017; doi:10.1152/ajpheart.00380.2017.

RESEARCH ARTICLE | *Mechanisms of Exercise-Induced Amelioration of Cardiovascular Disease*

Exercise facilitates early recognition of cardiac and vascular remodeling in chronic thromboembolic pulmonary hypertension in swine

Kelly Stam, Richard W. B. van Duin, André Uitterdijk, Zongye Cai, Dirk J. Duncker, and Daphne Merkus

Experimental Cardiology, Department of Cardiology, Thoraxcenter, Cardiovascular Research Institute COEUR, Erasmus Medical Center Rotterdam, Rotterdam, The Netherlands

Submitted 30 June 2017; accepted in final form 19 November 2017

Stam K, van Duin RW, Uitterdijk A, Cai Z, Duncker DJ, Merkus D. Exercise facilitates early recognition of cardiac and vascular remodeling in chronic thromboembolic pulmonary hypertension in swine. *Am J Physiol Heart Circ Physiol* 314: H627–H642, 2018. First published November 22, 2017; doi:10.1152/ajpheart.00380.2017.—Chronic thromboembolic pulmonary hypertension (CTEPH) develops in 4% of patients after pulmonary embolism and is accompanied by an impaired exercise tolerance, which is ascribed to the increased right ventricular (RV) afterload in combination with a ventilation/perfusion (V/Q) mismatch in the lungs. The present study aimed to investigate changes in arterial P_{O_2} and hemodynamics in response to graded treadmill exercise during development and progression of CTEPH in a novel swine model. Swine were chronically instrumented and received multiple pulmonary embolisms by *1*) microsphere infusion (Spheres) over 5 wk, *2*) endothelial dysfunction by administration of the endothelial nitric oxide synthase inhibitor N^{ω}-nitro-L-arginine methyl ester (L-NAME) for 7 wk, *3*) combined pulmonary embolisms and endothelial dysfunction (L-NAME + Spheres), or *4*) served as sham-operated controls (sham). After a 9 wk followup, embolization combined with endothelial dysfunction resulted in CTEPH, as evidenced by mean pulmonary artery pressures of 39.5 ± 5.1 vs. 19.1 ± 1.5 mmHg (Spheres, $P < 0.001$), 22.7 ± 2.0 mmHg (L-NAME, $P < 0.001$), and 20.1 ± 1.5 mmHg (sham, $P < 0.001$), and a decrease in arterial P_{O_2} that was exacerbated during exercise, indicating V/Q mismatch. RV dysfunction was present after 5 wk of embolization, both at rest (trend toward increased RV end-systolic lumen area, $P = 0.085$, and decreased stroke volume index, $P = 0.042$) and during exercise (decreased stroke volume index vs. control, $P = 0.040$). With sustained pulmonary hypertension, RV hypertrophy (Fulton index $P = 0.022$) improved RV function at rest and during exercise, but this improvement was insufficient in CTEPH swine to result in an exercise-induced increase in cardiac index. In conclusion, embolization in combination with endothelial dysfunction results in CTEPH in swine. Exercise increased RV afterload, exacerbated the V/Q mismatch, and unmasked RV dysfunction.

NEW & NOTEWORTHY Here, we present the first double-hit chronic thromboembolic pulmonary hypertension swine model. We show that embolization as well as endothelial dysfunction is required to induce sustained pulmonary hypertension, which is accompanied by altered exercise hemodynamics and an exacerbated ventilation/perfusion mismatch during exercise.

animal model; chronic thromboembolic pulmonary hypertension; exercise; right ventricular remodeling; vascular remodeling

INTRODUCTION

Pulmonary hypertension (PH) is a chronic pathophysiological disorder of the pulmonary vasculature and is defined as a chronic pulmonary arterial pressure (PAP) ≥ 25mmHg at rest for a consecutive period of at least 6 wk, although PAP ≥ 19 mmHg at rest is already associated with increased mortality at long term (26, 59). Treatment modalities for PH are very limited, and, even when treated, the disease often progresses to right heart failure and death. The World Health Organization differentiates five groups of PH, based on their etiology. Chronic thromboembolic PH (CTEPH), categorized as group 4, develops in ~4% of patients after acute pulmonary embolism and up to 10% of patients with recurrent pulmonary embolism (61, 65) and is defined as persistent PAP above 25 mmHg for over 6 mo (15). The obstructions in the pulmonary arteries increase pulmonary vascular resistance (PVR) and result in ventilation-perfusion (V/Q) mismatch in the lungs. The main treatment options for CTEPH are interventions to remove proximal obstructions in eligible patients such as pulmonary endarterectomy or balloon angioplasty (13, 17, 23). Moreover, it is increasingly being recognized that distal pulmonary vasculopathy, which is left untreated when removing only the proximal obstruction(s), contributes significantly to the increase in pulmonary vascular resistance (PVR) (16, 30, 38, 55). It is currently unknown when these distal vascular lesions develop and whether endothelial dysfunction promotes such development.

Dating back to 1984, many investigators have attempted to establish a solid large animal model to study the pathophysiology of CTEPH using different embolization algorithms and embolization materials, including air, autologous blood cloths, sephadex beads, and glue (Table 1). Although PAP increases acutely upon embolization in these models, most studies were unsuccessful in establishing a sustained level of elevated PAP during prolonged followup (1, 21, 31, 37, 39, 42, 43, 51, 53, 63, 66). Those studies that did report CTEPH during prolonged

Address for reprint requests and other correspondence: D. Merkus, Dept. of Experimental Cardiology, Erasmus MC, University Medical Center Rotterdam, PO Box 2040, Rotterdam 3000 CA, The Netherlands (e-mail: d.merkus@erasmusmc.nl).

Table 1. *Comparison between large animal studies using embolization techniques to create chronic thromboembolic pulmonary hypertension models*

Reference	Year of Publication	Species	Sex	Embolic Material	Number of Embolizations	Number of Animals	Anesthesia During Right Heart Catheterization	Recovery Period	Mean Pulmonary Artery Pressure, mmHg	Pulmonary Vascular Resistance, wood units	Right Ventricular Weight/(Left Ventricular Weight + Septum Weight)	Right Ventricular Function Assessment
Shelub et al. (53)	1984	Canine	Female	Sephadex G50	Variable (16−30 wk)	5	None	>7 days	29 (4)	8.3 (2.3)	0.54[e]	None
Perckett et al. (42)	1988	Sheep	NR	Air (continuous)	12 days	5	None	1.5 h	23 (2)[f]	5.2[f]	0.38 (0.06)	None
Moser et al. (39)	1991	Canine	NR	3−4 Venous thrombi	2	10	Halothane	32 days	20.3 (2)	4.2[a]	NR	None
Weimann et al. (63)	1999	Swine	Male	Sephadex G50 (15 mg/kg)	3	8	Ketamine	7 days	18 (3)	4.3[a,b]	NR	None
Kim et al. (31)	2000	Canine	NR	Ceramic beads (3 mm)	4	5	Halothane	6 mo	17 (2)	4.3[a]	NR	None
Zhou et al. (66)	2011	Sheep	Female	Air (continuous)	8 wk	4	None	7 days	34 (2.6)	4.5 (0.9)	0.36 (0.01)	None
Sage et al. (51)	2012	Swine	NR	Right pulmonary artery ligation	1	10	Pentobarbital	5 wk	16.2 (1.3)	10.05[c] (0.69)	NR	None
Pohlmann et al. (43)	2012	Sheep	NR	Sephadex G50 (~21.1 ± 0.5 g total)	60	9	None	1 day	35 (3)	1.7 (0.2)	0.42 (0.01)	None
Garcia-Alvarez et al. (18)	2013	Swine	Male	Sephadex G50	4 (3−6)	9	Midazolam	2 mo	27 (3)	2.2[d] (1.1)	NR	Cardiovascular magnetic resonance
Mercier et al. (37)	2013	Swine	NR	Histoacryl + left pulmonary artery ligation	5	5	NR	7 days	28.5 (1.7)	9.8[a]	NR	Echocardiography, computed tomography
Guihaire et al. (20)	2014	Swine	NR	Histoacryl + left pulmonary artery ligation	5	5	Isoflurane	6 wk	41 (4)	10.0[a,c]	NR	Echocardiography, pressure-volume loop
Guihaire et al. (21)	2015	Swine	NR	Histoacryl + left pulmonary artery ligation	5	13	Isoflurane	7 days	34 (9)	12.4[a,c]	NR	Echocardiography dobutamine, pressure-volume loop
Boulate et al. (5)	2015	Swine	Male	Histoacryl + left pulmonary artery ligation	5	5	NR	7 wk	27 (1.1)	7.9 (0.6)	NR	None
Aguero et al. (1)	2015	Swine	Female	Sephadex G50 (20 mg/kg)	6	6	Propofol	14 days	16 (2)	1.5[b]	0.41 (0.02)	Echocardiography
Aguero et al. (1)	2015	Swine	Female	Sephadex G50 (20 mg/kg) + coiling	4	6	Propofol	1 mo	23 (4)	1.6[b]	0.47 (0.06)	Echocardiography
Tang et al. (58)	2015	Canine	NR	Autologous thrombi (0.3 × 1 cm)	NR	13	Propofol	14 days	25.2 (3.6)	NR	NR	Dual-energy computed tomography
Rothman et al. (50)	2017	Swine	Female	Ceramic beads (0.6−0.9 mm)	21−40	3	Isoflurane	NR	36.6 (0.9)[g]	NR	NR	None
Rothman et al. (50)	2017	Canine	Female	Ceramic beads (0.6−0.9 mm)	9−12	3	Isoflurane	20 mo[h]	47[g]	7.8	NR	None
Present study		Swine	Male + female	Polyethylene spheres (600−710 μm, ~9,000 per embolization)	4 (2−5)	6	None	4–5 wk	39.5 (5.1)	7.8 (3.4)	0.51 (0.03)	Echocardiography, cardiopulmonary exercise testing

NR, not reported. [a]Calculated from $dyn \cdot s^{-1} \cdot cm^{-5}$. [b]Calculated from the pulmonary vascular resistance index. [c]Total pulmonary vascular resistance. [d]Median (interquartile range) reported. [e]Only reported 2 of 5 cases. [f]Calculated from cmH_2O or cmH_2O/l. [g]Systolic pulmonary artery pressure. [h]Only reported one animal.

followup (5, 18, 20, 50) have in common that they used repeated (between 4 and 40 times) embolization procedures, thereby obstructing a significant fraction of the pulmonary vasculature. In those studies, PAP also decreased between embolization procedures, but a gradual increase in PAP occurred over time. However, most studies did not determine whether this gradual increase in PAP was solely due to the progressive embolization of pulmonary vessels or that distal pulmonary microvasculopathy also developed. Recent findings by Boulate et al. (5) suggest that distal vasculopathy was present in their model of left pulmonary artery ligation in combination with glue embolizations. However, in the latter study, as in most of the aforementioned studies, hemodynamic measurements were performed under anesthesia, which may have influenced cardiac function and pulmonary hemodynamics (4, 9, 49). Moreover, in none of these studies, pulmonary hemodynamics were assessed during exercise.

The increased PVR imposes an increased afterload on the right ventricle (RV). As contractile reserve of the RV is limited (22), PH results in subacute RV dilation and dysfunction (55). With sustained PH, the RV undergoes structural remodeling and hypertrophy (55). Although RV remodeling is initially beneficial and helps the RV to cope with the increased afterload, it poses a risk factor for the later development of RV failure. Evaluation of RV function during stress has been shown to be of prognostic value in patients (24, 25, 48). RV dysfunction is exacerbated during exercise, when cardiac demand increases and the RV is required to pump more blood against an increased afterload. Therefore, RV functional measurements during stress enable the evaluation of the capacity of the RV to cope with an increased afterload and facilitate early detection of RV dysfunction (52). In addition to RV dysfunction, V/Q mismatch is thought to contribute to the exercise intolerance observed in patients with CTEPH (7, 8, 48). To date, however, studies describing animal models of CTEPH have not evaluated the occurrence of V/Q mismatch at rest and during exercise.

In light of these considerations, we developed and characterized a clinically relevant swine model of PH type 4, using a double-hit (endothelial dysfunction in conjunction with repeated embolizations) approach, in which we applied treadmill exercise as a physiological stressor to evaluate the function of the RV in the development and progression of CTEPH.

METHODS

Experiments were performed in accordance with the "Guiding Principles in the Care and Use of Laboratory Animals" as approved by the Council of the American Physiological Society and with approval of the Animal Care Committee of the Erasmus Medical Center Rotterdam (3158, 109-13-09). Twenty-four Yorkshire × Landrace swine (2–3 mo old, 21.5 ± 0.9 kg at the time of surgery) of either sex entered the study. Eighteen animals completed the protocol, as six animals were excluded due to complications: two animals due to infections, two animals due to catheter failure, and two animals due to acute cardiopulmonary failure after CTEPH induction. An overview of the experimental protocol is shown in Fig. 1.

Surgery. Surgical details have been extensively described previously (10). In short, swine were sedated with an intramuscular injection of tiletamine-zolazepam (5 mg/kg, Virbac, Barneveld, The Netherlands), xylazine (2.25 mg/kg, AstFarma, Oudewater, The Netherlands), and atropine (1 mg, Teva Nederland, Haarlem, The Netherlands), intubated, and ventilated with a mixture of O_2 and N_2 [1:2 (vol/vol)], to which 2% (vol/vol) isoflurane was added to maintain anesthesia. Under sterile conditions, the chest was opened via a left thoracotomy in the fourth intercostal space, and fluid-filled polyvinylchloride catheters (B Braun Medical, Bethlehem, PA) were placed in the RV, pulmonary artery, aorta, and left atrium for blood sampling and measurement of pressures. A flow probe (Transonic Systems, Ithaca, NY) was positioned around the ascending aorta for the measurement of cardiac output (CO). Catheters were tunneled to the back, and animals were allowed to recover for 1 wk while receiving analgesia [0.015 mg/kg buprenorphine im and a slow-release transdermal fentanyl patch (12 μg/h) for 48 h, Indivior, Slough, UK] on the day of surgery and daily antibiotic prophylaxis (25 mg/kg amoxicillin iv, Centrafarm, Etten-Leur, The Netherlands) for 7 days.

CTEPH induction. Four groups of animals were studied. In the first group (Spheres group; $n = 3$), multiple injections of fluorescent blue polyethylene microspheres [diameter: 600–710 μm (maximal microsphere size that did not cause clogging of the catheter), density: 1.134 g/ml, UVPMS-BB-1.13, Cospheric, Santa Barbara, CA] were given. Microspheres (500 mg, corresponding to ~2,500 microspheres) were suspended in 50 ml of autologous blood with 0.5 ml of 5,000 IU heparin added and slowly infused into the RV while PAP was monitored. Microsphere infusions were repeated until PAP reached ~60 mmHg or when arterial P_{O_2} dropped below ~40 mmHg, measured 30 min after infusion at rest or a maximum of 3 g (~15,000) microspheres were infused. In the subsequent 4 wk, microsphere infusions were repeated. In the first animal, embolization procedures were performed multiple times per week, whereas in the subsequent two animals, embolization procedures were performed once a week. As no sustained PH was induced with this protocol, in the second group ($n = 6$), multiple injections of microspheres were combined with a daily bolus infusion of the endothelial nitric synthase synthase (eNOS) inhibitor N^{ω}-nitro-L-arginine methyl ester (L-NAME; Enzo Life Sciences) to mimic endothelial dysfunction often present in CTEPH patients. L-NAME is converted to its active metabolite N^{ω}-nitro-L-arginine within 19 min, with the half-life of N^{ω}-nitro-L-arginine amounting to ~20 h (62). On the first day, animals were given L-NAME (10 mg/kg iv) as a bolus infusion. On subsequent days, the dose of L-NAME was increased by 10 $mg \cdot kg^{-1} \cdot day^{-1}$ up to 30 mg/kg iv, which was maintained until 2 wk before the end of the study (34, 45). Four days after the first L-NAME administration, hemodynamic measurements were performed as described above, and microspheres were then infused into the RV as described above for *group 1*. In the subsequent 4 wk, microsphere infusion was performed at weekly intervals if PAP was <25 mmHg and/or arterial P_{O_2} was >70 mmHg, as described above. During the final 4 wk of followup, no microsphere infusions were performed.

The third group of animals did not receive L-NAME or microspheres (sham group; $n = 4$), and the fourth group was given chronic L-NAME but no microspheres were infused (L-NAME group; $n = 5$).

Exercise protocol. Experiments were performed 1–9 wk after surgery. Catheters were connected to fluid-filled pressure transducers (Combitrans, B. Braun Medical) positioned on the back of the animals and calibrated at midchest level. With swine standing quietly, resting hemodynamic measurements, consisting of CO, aortic blood pressure (MAP), PAP, left atrial pressure, and RV pressure, were obtained, and arterial and mixed venous blood samples were taken. Hemodynamic measurements and blood gas sampling were repeated during a graded exercise protocol, with swine running on a motor-driven treadmill (10, 12). During the embolization period, exercise was performed just before the weekly injection of microspheres and/or L-NAME. Swine were subjected to a four-stage exercise protocol (1–4 km/h). Hemodynamic variables were continuously recorded, and blood samples were collected during the last 60 s of each 3-min exercise stage, when hemodynamic steady state had been reached. Measurements of arterial and mixed venous P_{O_2} (in mmHg), P_{CO_2} (in mmHg), oxygen saturation (in %), hemoglobin concentration (in g/dl), and lactate (in mmol/l) were immediately performed with a blood gas analyzer (ABL 800, Radiometer Medical ApS, Brønshøj, Denmark) (10, 12).

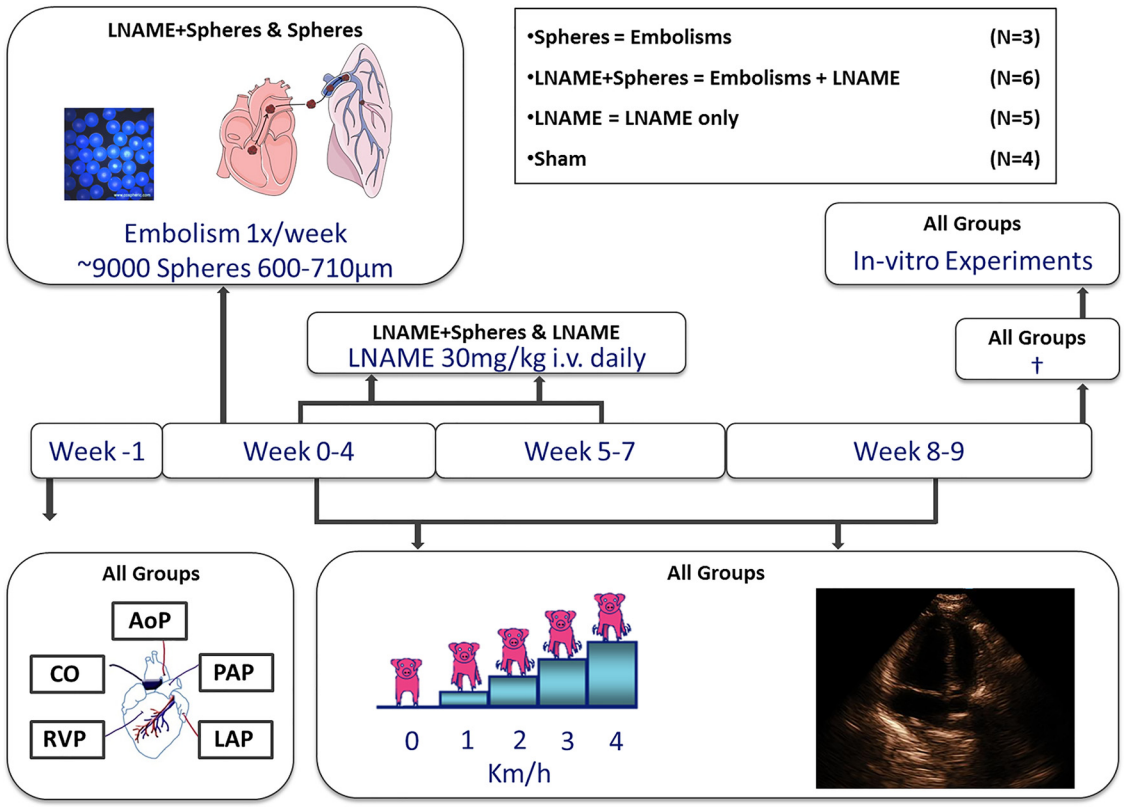

Fig. 1. Experimental protocol. Catheters were placed in the aorta, right ventricle (RV), pulmonary artery (PA), and left atrium (LA) for blood sampling and measurement of pressures, and a flow probe was positioned around the ascending aorta for measurement of cardiac output (CO). The endothelial nitric oxide synthase inhibitor N^{ω}-nitro-L-arginine methyl ester (L-NAME) was administered intravenously in both L-NAME and L-NAME + microsphere infusion (Spheres) groups until 2 wk before euthanasia. Embolization procedures were performed in the awake state in the Spheres and L-NAME + Spheres group from *week 2* until *week 5*. All animals performed the treadmill exercise protocol, and RV function was echocardiographically determined weekly in the awake state. At the end of the followup (*week 9–10*), all animals were euthanized, and in vitro experiments were performed. AoP, aortic pressure; RVP, RV pressure; PAP, pulmonary artery pressure; LAP, left atrial pressure.

Echocardiography. During the entire followup period, RV dimensions and tricuspid annular plane systolic excursion (TAPSE) were assessed weekly using echocardiography (ALOKA ProSound SSD-4000, Hitachi Aloka Medical, Japan) under awake resting conditions. An apical four-chamber view was obtained for the determination of RV end-diastolic cross-sectional lumen area and end-systolic cross-sectional lumen area, whereas TAPSE was determined using M-mode in the four-chamber view.

Euthanization. After the experimental protocols were completed, animals were sedated and intubated as described before. With animals ventilated under deep anesthesia [pentobarbital sodium (6–12 $mg \cdot kg^{-1}\ h^{-1}$)], a sternotomy was performed. The heart was arrested and immediately excised together with the lungs. To assess relative RV hypertrophy, the heart was sectioned into the RV and the left ventricle including the septum (LV) and weighed, and RV hypertrophy was assessed using the Fulton index (RV/LV). Myograph experiments were performed on isolated pulmonary small arteries (diameter: ~300 µm) (11, 40). Pulmonary small arteries were dissected and stored overnight in cold oxygenated (95% O_2-5% CO_2) Krebs bicarbonate solution [containing (in mM) 118 NaCl, 4.7 KCl, 2.5 $CaCl_2$, 1.2 $MgSO_4$, 1.2 KH_2PO_4, 25 $NaHCO_3$, and 8.3 glucose; pH 7.4]. The next day, the dissected vessels were cut into segments of ~2 mm in length, mounted in microvascular myograph baths (Danish MyoTechnology, Aarhus, Denmark) containing 6 ml of Krebs bicarbonate solution aerated with 95% O_2-5% CO_2, and maintained at 37°C. The internal diameter was set to a tension equivalent of 0.9 times the estimated diameter at 20-mmHg effective transmural pressure. Changes in contractile force were recorded with a Harvard isometric transducer. Vessels were subsequently exposed twice to 30 mM KCl. Endothelial function was measured by observing dilation to 10 nM substance P after preconstriction with 100 nM of the stable thromboxane A_2 analog 9,11-dideoxy-11α,9α epoxymethanoprostaglandin $F_{2\alpha}$ (U-46619).

Histology. The accessory lobe of the right lung was first flushed with physiological saline (0.9% NaCl) through the main bronchus, to clear the airways from sputum and surfactant, at a constant physiological pressure of 25 cmH_2O. Subsequently, the lobe was fixed by tracheal installation of 3.5–4% buffered formaldehyde at a constant physiological pressure of 25 cmH_2O for a minimum of 24 h with the lobe submerged in fixative (33). Transverse sections were obtained from the tip, middle, and base of the fixed accessory lobe for histology. All sections were processed and embedded in paraffin wax. Paraffin sections of 4.5 µm were cut and stained with Resorcin Fuchsin von Gieson. These sections were evaluated by light microscopy using the Hamamatsu NanoZoomer Digital Pathology (NDP) slide scanner (Hamamatsu Nanozoomer 2.0HT, Hamamatsu Photonics K.K., Hamamatsu City, Japan). Morphometric measurements of pulmonary arteries were performed using the NDP viewer (Hamamatsu Photonics K.K.). To ensure that pulmonary veins were excluded from analysis, vessels in close proximity to the septae were excluded from analysis. Only transversely cut vessels of predetermined diameters (<50 µm) were analyzed. Assuming circularity of the vessels, inner and outer radii (r) were calculated as follows: r = perimeter/2 × π. Wall thickness was calculated as follows: outer radius – inner radius.

A section of the RV was processed and embedded in paraffin wax. Paraffin sections of 4.5 μm were cut and stained with Gomori staining. Only transversely cut cardiomyocytes were analyzed for cross-sectional area using the NDP viewer.

Quantitative PCR. For the detection of interleukin (IL)-6, tumor necrosis factor-α (TNF-α), transforming growth factor-β1 (TGF-β_1), angiopoietin 1 (Ang-I), angiopoietin 2 (Ang-2), Ang-1 receptor (TIE-2), vascular endothelial growth factor (VEGF)-A, VEGF receptor 1 (FLT-1), and VEGF receptor 2 (KDR) mRNA, lung tissue was snap frozen in liquid nitrogen after excision. Small pieces of tissue (<30 mg) were homogenized by adding RLT lysisbuffer (Qiagen, Venlo, The Netherlands) and 2-mercaptoethanol (Sigma-Aldrich, Zwijndrecht, The Netherlands) using a homogenizer. After proteinase K (Invitrogen, Breda, The Netherlands) treatment at 55°C for 10 min, total RNA was isolated using the RNeasy Fibrous Tissue Mini Kit (Qiagen). RNA was eluted in RNase-free water, and the concentration was determined using a NanoDrop (NanoDrop1000, ThermoFisher Scientific, Bleiswijk, The Netherlands). RNA integrity was confirmed with a Bioanalyzer (2100 Bioanalyzer, Agilent, Santa Clara, CA). cDNA was synthesized from 500 ng total RNA with SensiFAST cDNA Synthesis Kit (Bioline, London, UK). Quantitative PCR (CFX-96, Bio-Rad, Hercules, CA) was performed with a SensiFAST SYBR and Fluorescein Kit (Bioline, London, UK). Target gene mRNA levels were normalized against β-actin, GADPH, and cyclophilin using the CFX manager software (Bio-Rad). Relative gene expression data were calculated using the $\Delta\Delta C_T$ method, where C_T is threshold cycle. All primer sequences are shown in Table 2.

Data analysis and statistics. Echocardiographic data were analyzed using a DICOM viewer (Rubo Medical Imaging, Aerdenhout, The Netherlands) and SigmaScan Pro (Systat Software, San Jose, CA). Three images of end diastole, three images of end systole, and three TAPSE recordings per echo were selected in the DICOM viewer. RV lumen area and TAPSE length were manually drawn per image, automatically calculated in SigmaScan, and then averaged per animal per time point.

Digital recording and offline analysis of hemodynamic data were performed with MatLab (MathWorks, Natick, MA) and have been previously described in detail (12, 57). To account for growth, CO was corrected for body weight, resulting in cardiac index (CI). The total pulmonary vascular resistance index (tPVRi) and systemic vascular resistance index (SVRi) were calculated as PAP divided by CI and MAP divided by CI, respectively. The body oxygen consumption index was calculated as the product of CI and the difference between arterial and mixed venous oxygen content of the blood.

Statistical analysis was performed using SPSS (version 21.0, IBM, Armonk, NY). Differences between Spheres, L-NAME + Spheres, L-NAME, and sham groups over time and at rest were analyzed with two-way multivariate ANOVA with PAP, tPVRi, CI, and stroke volume index (SVi) as dependent variables and time and group as independent factors. Post hoc analyses was performed using Bonferroni corrections. As no differences were observed in hemodynamics, oxygenation, histology, inflammation, and angiogenesis among sham, L-NAME, and Spheres groups, these groups were pooled into a single control group for subsequent analyses. Echocardiography data and Fulton index were analyzed by one-way multivariate ANOVA with the RV end-systolic cross-sectional lumen area, RV end-diastolic cross-sectional lumen area, RV fractional area change (RVFAC), TAPSE, cross-sectional area, RV weight/LV weight, and RV weight/body weight as dependent variables and group as independent factor. The difference in effect of exercise on the hemodynamic parameters between L-NAME + Spheres and control groups at the same time point were assessed by two-way repeated-measures ANOVA with exercise as within-subject factor and group as between-subject factor. The difference in effect of exercise on hemodynamic parameters compared with baseline within the individual groups was assessed with two-way repeated-measures ANOVA with exercise as within-subject factor and time as between-subject factor. Statistical significance was accepted when $P \leq 0.05$. Data are presented as means ± SE.

RESULTS

Induction and progression of CTEPH. To induce CTEPH, microspheres (600–710 μm) were infused slowly into the RV. In the Spheres group, one animal received 25 embolizations with an average of 2,700 microspheres/embolization procedure. The two other animals underwent five embolization procedures with an average of 9,200 microspheres/embolization procedure. Each microsphere has a cross-sectional area of 2.5–4.7 × 10^{-14} m^2, a volume of 1.1–1.8 × 10^{-10} m^3, and a total surface area of 1.0–1.9 × 10^{-13} m^2. With an average of 36,000 spheres/animal, this results in a total cross-sectional area of 9.1–17.0 × 10^{-10} m^2, a total volume of 4.1–6.5 × 10^{-6} m^3, and a total surface area of 3.7–6.8 × 10^{-9} m^2. Although immediately after injection a substantial increase in PAP was observed, this increase waned over the course of the next few days, such that with weekly measurements, resting PAP and tPVRi did not increase significantly over time in these animals (PAP being 21.0 ± 1.8 mmHg and tPVRi being 100 ± 4 mmHg·min·l^{-1}·kg at baseline and 19.1 ± 1.5 mmHg and 147 ± 22 mmHg·min·l^{-1}·kg, respectively, at *week 9*).

In the second group (L-NAME + Spheres), an average of four embolization procedures (range between 2 and 5) were required to induce chronic PH. The number of microspheres infused per embolization procedure did not change over time, being 9,000 ± 400.

In these animals, resting PAP increased gradually over time (from 21.8 ± 1.1 mmHg at baseline before L-NAME to

Table 2. *Primer sequences used for quantitative PCR*

Genes	Forward Primer	Reverse Primer
IL-6	5′-CTCCAGAAAGAGTATGAGAGC-3′	5′-AGCAGGCCGGCATTTGTGGTG-3′
TNF-α	5′-TGCACTTCGAGGTTATCGGCC-3′	5′-CCACTCTGCCATTGGAGCTG-3′
TGF-β1	5′-GTGGAAAGCGGCAACCAAAT-3′	5′-CACTGAGGCGAAAACCCTCT-3′
Ang-1	5′-AATGGACTGGGAAGGAAACCG-3′	5′-TCTGTTTTCCTGCTGTCCCAC-3′
Ang-2	5′-AGGCAACGAGGCTTACTCAC-3′	5′-TCGTTGTCTGCGTCCTTTGT-3′
TIE-2	5′-GTCCCGAGGTCAAGAAGTGT-3′	5′-AAGGGGTGCCACCTAAGCTA-3′
VEGF-A	5′-ACTGAGGAGTTCAACATCGCC-3′	5′-CATTTACACGTCTGCGGATCTT-3′
FLT-1	5′-AAGGAGGGCGTGAGGATGAGG-3′	5′-GGCTTGCAGCAGGTCGCCTAG-3′
KDR	5′-TTCTCCGAGCTGGTGGAGCAC-3′	5′-AGGTAGGCAGAGAGAGTCCGG-3′

IL-6, interleukin-6; TNF-α, tumor necrosis factor-α; TGF-β_1, transforming growth factor-β_1; Ang-1, angiopoietin 1; Ang-2, angiopoietin 2; TIE-2, Ang-1 receptor; VEGF-A, vascular endothelial growth factor A; FLT-1, vascular endothelial growth factor receptor 1; KDR, vascular endothelial growth factor receptor 2.

32.2 ± 3.1 mmHg at *week 5* and 39.5 ± 5.1 mmHg at *week 9*) as a result of a progressive increase in tPVRi (Fig. 2). The increase in tPVRi in L-NAME + Spheres animals was due to vascular obstructions by the injected spheres in combination with remodeling and dysfunction of the pulmonary microvessels. The latter was reflected by an increased wall thickness (Fig. 4) and impaired vasorelaxation in response to substance P in isolated pulmonary small arteries (86 ± 3%, 82 ± 3%, 90 ± 2%, and 62 ± 8% in sham, L-NAME, Spheres, and L-NAME + Spheres groups, $P < 0.05$ vs. all other groups). Histologically, microspheres in the lungs were surrounded by fibrous tissue; however, quantitative PCR analysis revealed no changes in the inflammatory markers IL-6, TNF-α, and TGF-β_1 (Fig. 5). Moreover, expression of the angiogenic factors VEGF-A, Flt-1, and KDR as well as Ang-1, Ang-2, and Tie-2 were also not different between groups (Fig. 5).

Although acute L-NAME administration did result in a small increase in PAP and tPVRi within the first 30 min, both at baseline (PAP: 17.3 ± 0.9 to 21.0 ± 2.1 mmHg and tPVRi: 101 ± 14 to 137 ± 17 mmHg·min·l^{-1}·kg) and after 5 wk of L-NAME administration (PAP: 17.6 ± 1.8 to 21.9 ± 2.2 mmHg and tPVRi: 120 ± 6 to 150 ± 18 mmHg·min·l^{-1}·kg), PAP and tPVRi normalized before the next injection. Thus, in the L-NAME group, PAP did not significantly increase over time, being 18.0 ± 1.4 mmHg at *week 1* and 22.7 ± 2.0 mmHg at *week 9*, which was not significantly different from PAP in the sham group (17.5 ± 1.2 mmHg at baseline and 20.1 ± 1.5 mmHg at *week 9*; Fig. 2). As there were no sustained differences in hemodynamics, oxygenation, histology, inflammation, and angiogenic markers between the Spheres, L-NAME, and sham groups (Fig. 2, Fig. 3, Fig. 4, and Fig. 5), these groups were pooled into one control group for the remainder of the analyses.

RV function and hypertrophy. Echocardiography showed that RV diastolic and systolic lumen areas increased over time, whereas TAPSE tended to increase and RVFAC remained constant in the control group, reflecting growth of the RV over time (Fig. 6). Repeated microsphere injections over 5 wk in the L-NAME + Spheres group resulted in a trend toward higher end-systolic ($P = 0.085$) but not end-diastolic RV lumen area ($P = 0.15$), indicating mild RV contractile dysfunction. This was associated with a slight decrease in SVi compared with baseline, whereas RVFAC and TAPSE did not change. With sustained PH, SVi was reduced compared to baseline, but neither SVi nor RV diastolic and systolic lumen area and RVFAC were significantly different from the control group, although TAPSE showed a trend toward a reduction, indicating that resting RV function recovered. The Fulton index (RV weight/LV weight) and RV weight/body weight, measured at euthanasia after sustained PH, were significantly higher in L-NAME + Spheres swine compared with control swine, implying RV hypertrophy due to chronic PH (Fig. 6).

Exercise response. As CTEPH is accompanied by exercise intolerance due to both the increase in RV afterload and V/Q mismatch in the lungs, the response to exercise was examined in the initial phase after embolization [at 5 wk, referred to as "after microspheres" (AM) in the figures] and at the end of followup (8–9 wk after the first microsphere injection, referred

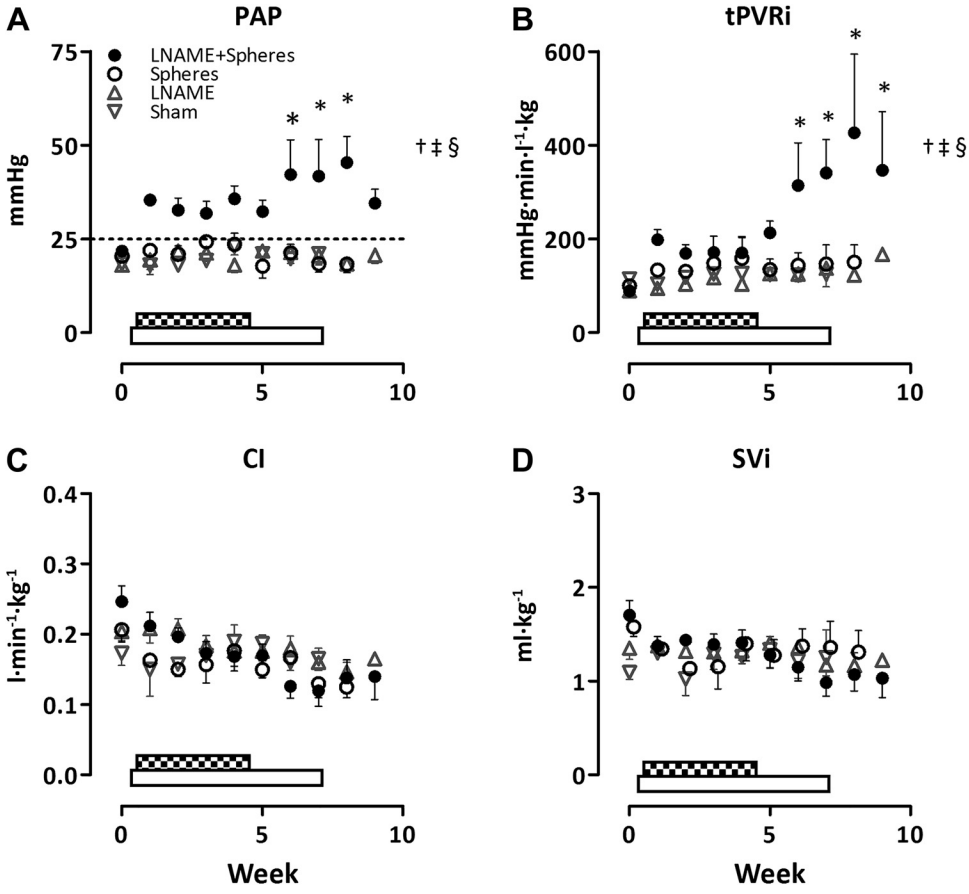

Fig. 2. Changes in pulmonary hemodynamics over time. The checkered bar indicates the period of weekly embolizations with microspheres (Spheres); the open bar indicates the administration time of N^{ω}-nitro-L-arginine methyl ester (L-NAME). Note that all baseline measurements were taken before the administration of L-NAME and/or Spheres. *A*: mean pulmonary arterial pressure (PAP). *B*: total pulmonary vascular resistance index (tPVRi). *C*: cardiac index (CI). *D*: stroke volume index (SVi). Data are means ± SE; $n = 4$ in the sham group, $n = 5$ in the L-NAME group, $n = 3$ in the Spheres group, and $n = 6$ but $n = 5$ in the L-NAME + Spheres group from *week 7* due to death of one animal caused by acute cardiopulmonary failure. *$P < 0.05$ vs. baseline (before the start of L-NAME and/or Spheres); †$P < 0.05$, L-NAME + Spheres vs. sham; ‡$P < 0.05$, L-NAME + Spheres vs. L-NAME; §$P < 0.05$, L-NAME + Spheres vs. Spheres and sham vs. L-NAME vs. Spheres not significant (NS).

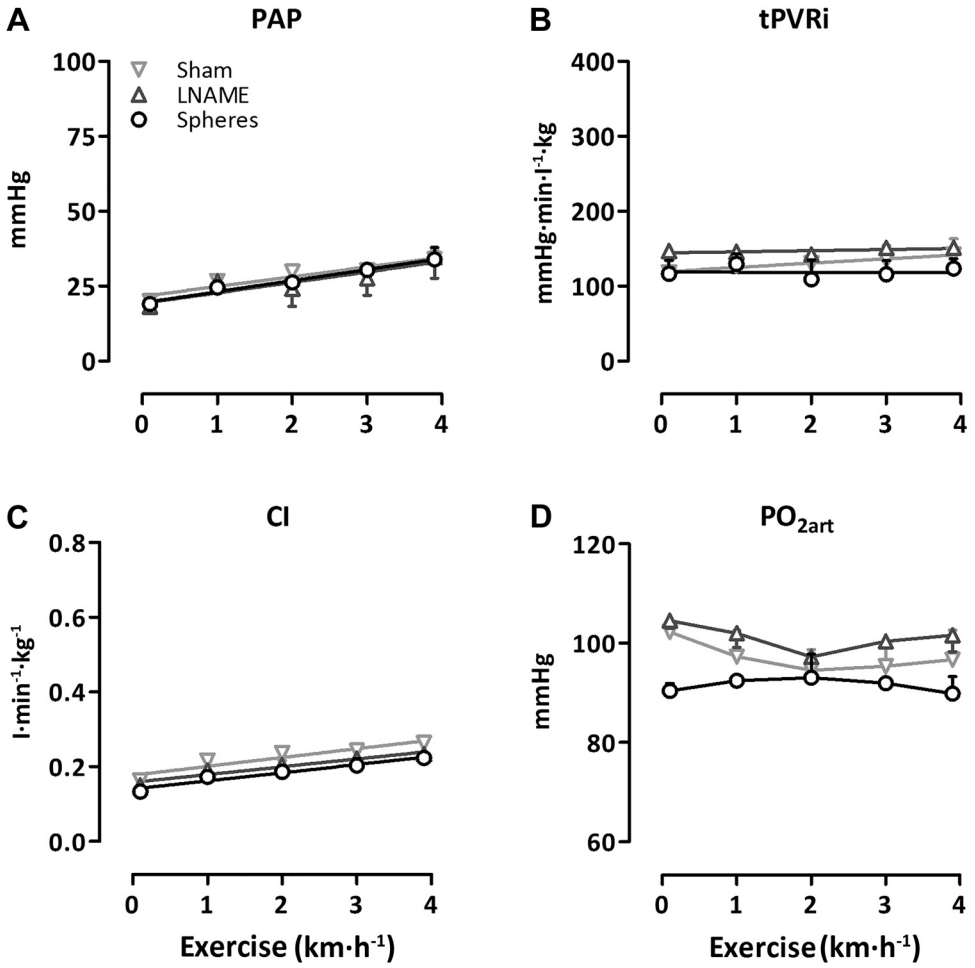

Fig. 3. Changes in pulmonary and cardiac hemodynamics with incremental levels of exercise at the end of followup of different control groups. Shown is the effect of exercise on mean pulmonary arterial pressure (PAP; *A*), total pulmonary vascular resistance index (tPVRi; *B*), cardiac index (CI; *C*), and arterial P_{O_2} ($P_{O_{2art}}$; *D*). Data are means ± SE; $n = 4$ in the sham group, $n = 5$ in the N^{ω}-nitro-L-arginine methyl ester (L-NAME) group, and $n = 3$ in the microsphere infusion (Spheres) group. No significant differences were observed.

to as "End" in the figures] and compared with the pooled control group at the corresponding time points. Graded treadmill exercise resulted in an increase in PAP at all time points in both L-NAME + Spheres and control animals (Fig. 7).

In L-NAME + Spheres animals, PAP was increased compared with its baseline measurement as well as compared with control animals at the corresponding time point in the initial phase after embolization (*week 5*), and the exercise-induced increase in PAP was exacerbated due to the significant elevation in tPVRi (Fig. 7). This increase in tPVRi was also reflected in the significantly higher slope of the relation between CI and PAP (Fig. 8). The exercise-induced increase in CI was attenuated in the L-NAME + Spheres group, which was due to a significant decrease in SVi during exercise (Fig. 7), as the exercise-induced increase in heart rate was not different between L-NAME + Spheres and control animals (Table 3). These observations indicate that the RV could not cope with the increased afterload during exercise in the initial phase after embolizations. At the end of the followup period, PAP was still elevated compared with both baseline and control. Moreover, the exercise-induced increase in CI was attenuated, whereas the exercise-induced increase in PAP was exacerbated at the end of the followup period in the L-NAME + Spheres group compared with the control group (Fig. 7). This translated into a persistent elevation of the slope of the relation between CI and PAP compared with control (Fig. 8), reflecting the sustained increase in tPVRi (Fig. 7). Interestingly, although SVi was still depressed at the end of followup, the exercise-induced decrease in SVi that was observed at AM was no longer present at the end of followup. The significant RV hypertrophy and recovery of RV function as assessed with echo, in conjunction with the blunted exercise-induced decrease of SVi compared with the initial phase after embolization, could be interpreted to suggest that RV hypertrophy served to restore RV function in the face of an increase in afterload.

Arterial P_{O_2} was lower in L-NAME + Spheres swine compared with control swine after the embolization phase and at the end of followup. Moreover, arterial P_{O_2} decreased more during exercise in L-NAME + Spheres swine compared with control swine at both time points. After the embolization phase, body oxygen extraction at rest was increased in the L-NAME + Spheres group compared with both baseline and the control group. The increased oxygen extraction compensated for the decreases in CI and arterial oxygenation, so that body oxygen consumption was unaltered. At the end of followup, the increase in body oxygen extraction was insufficient to compensate for the decrease in arterial P_{O_2}, and the oxygen consumption was lower at rest (Fig. 9). Although there was no difference in the exercise-induced increase in oxygen extraction, the exercise-induced increase in oxygen consumption was significantly attenuated both after the initial embolization phase (AM) and at the end of followup in L-NAME + Spheres

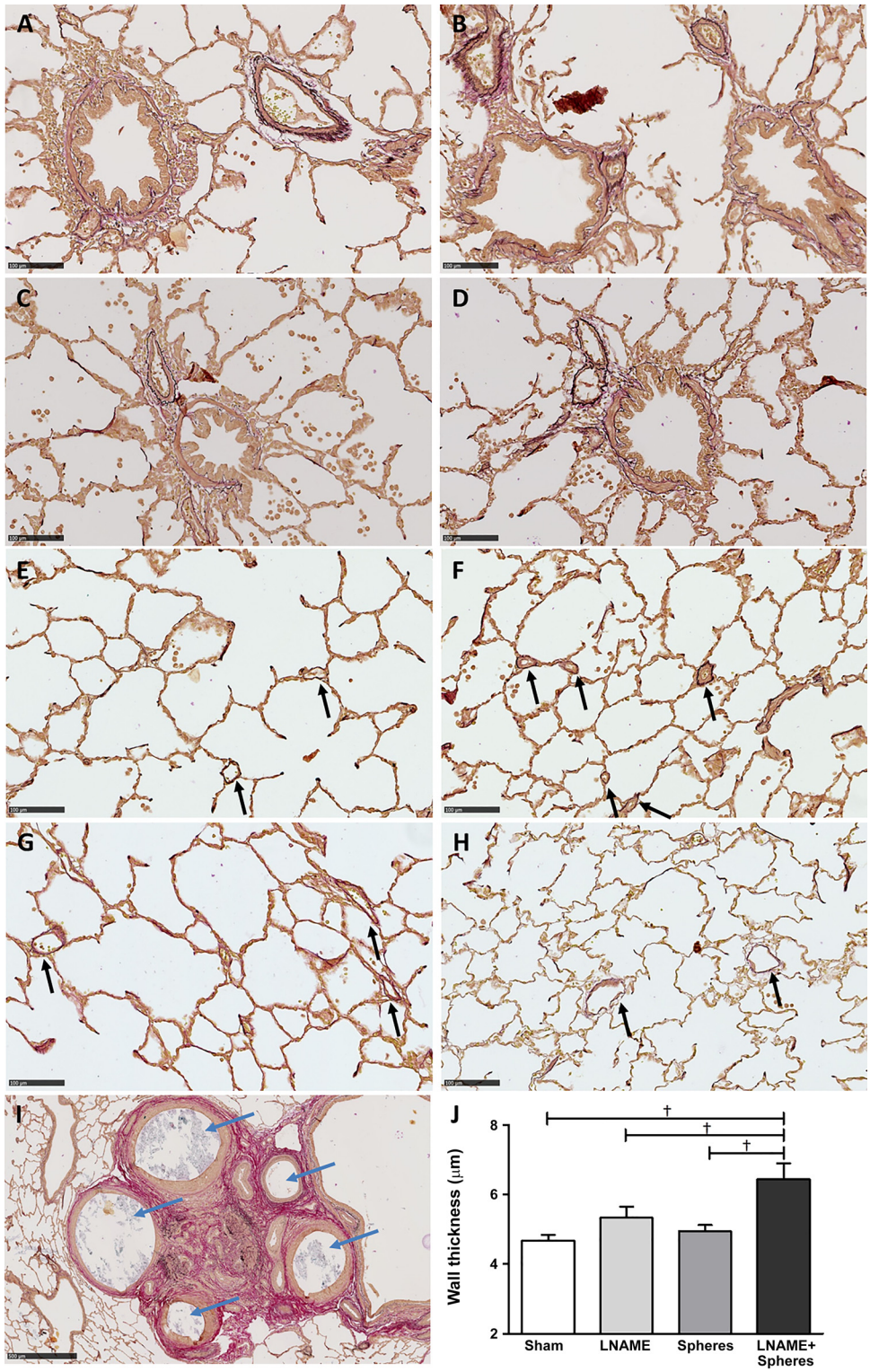

Fig. 4. Histological overview of lung tissue stained with Resorcin Fuchsin von Gieson. *A*−*D*: typical examples of bronchi with arteries of animals from the following groups: microsphere infusion (Spheres; *A*) nitro-L-arginine methyl ester (L-NAME + Spheres; *B*), L-NAME (*C*), and sham (*D*) groups are shown. Magnification: ×20. *E*–*H*: pulmonary microvessels adjacent to alveoli in swine from the following groups: Spheres (*E*), L-NAME + Spheres (*F*), L-NAME (*G*), and sham (*H*). Magnification: ×20. In L-NAME + Spheres lung tissue, microvessels presented with a thickened/muscularized wall (black arrows). *I*: example of occluded vessels due to the microspheres (blue arrows) surrounded by remodeled small unobstructed vessels in swine that received L-NAME + Spheres. *J*: quantitative presentation of the microvascular remodeling. The wall of microvessels (diameter < 50 μm) in the L-NAME + Spheres group were thickened compared with all other groups. Data are means ± SE; $n = 4$ in the sham group, $n = 3$ in the Spheres group, $n = 5$ in the L-NAME group, and $n = 6$ in the L-NAME + Spheres group. †$P < 0.05$ vs. the L-NAME + Spheres group. Scale bars = 100 μm in *A*-*H* and 500 μm in *I*.

animals compared with control animals, reflecting the attenuated increase in CI.

DISCUSSION

The main findings of this present study are that *1*) induction of CTEPH with a sustained increase in PAP and tPVRi over time required a combination of endothelial dysfunction (L-NAME) and repeated embolization procedures, as either stimulus alone did not result in a sustained increase in PAP or tPVRi; *2*) PAP and tPVRi were still increased up to 5 wk after the last embolization and 2 wk after the last L-NAME injection, consistent with sustained PH; *3*) development of CTEPH is accompanied by a decrease in arterial P_{O_2} during exercise both in the early phase after embolizations and at the end of

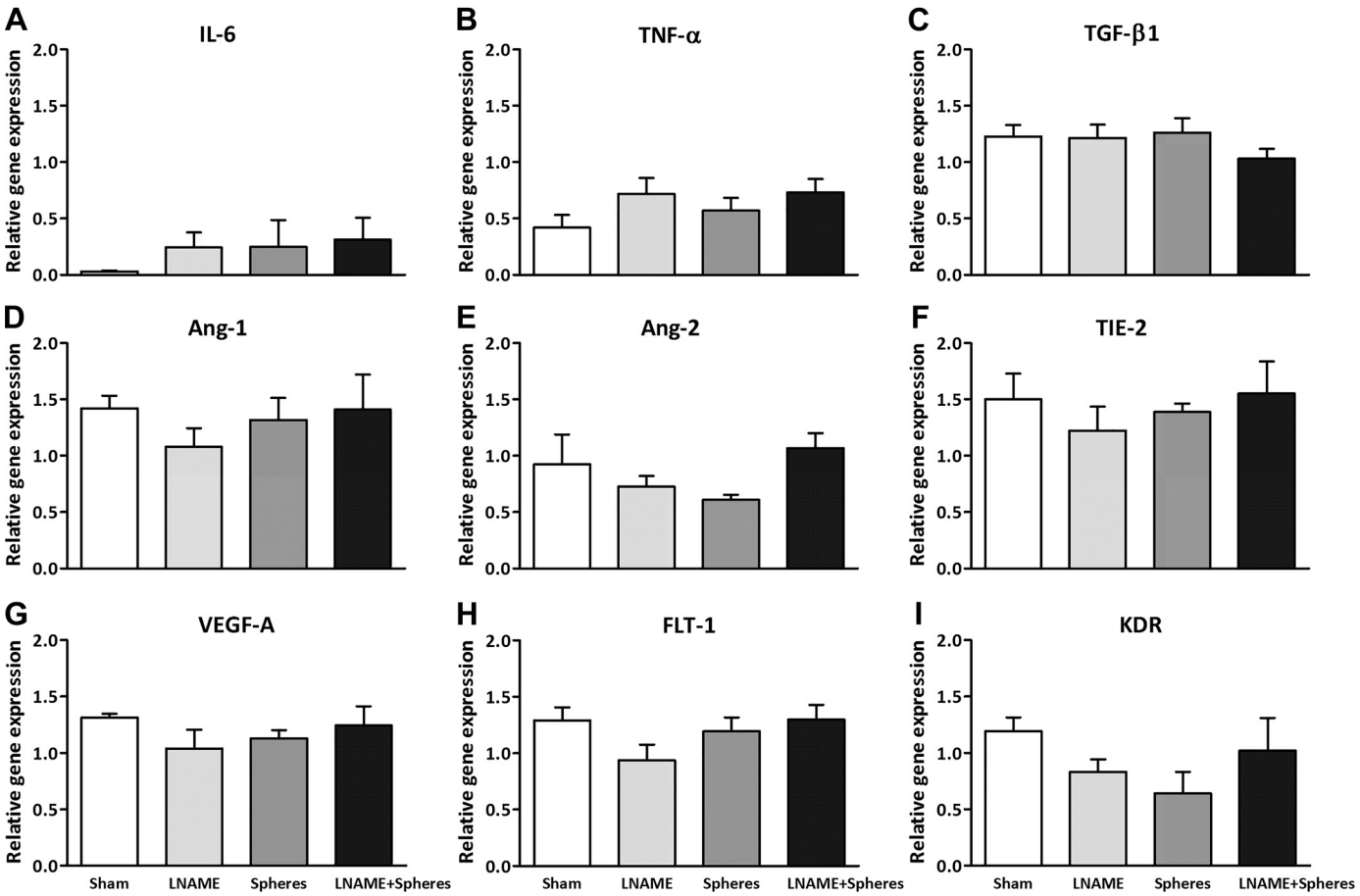

Fig. 5. Quantitative PCR. *A*−*I*: inflammatory (*A*–*C*) and angiogenic (*D*–*I*) gene expression in lung tissue of all experimental groups at the end time point of interleukin-6 (IL-6; *A*), tumor necrosis factor-α (TNF-α; *B*), transforming growth factor-β_1 (TGF-β_1; *C*), angiopoietin 1 (Ang-1; *D*), angiopoietin 2 (Ang-2; *E*), Ang-1 receptor (TIE-2; *F*), vascular endothelial growth factor (VEGF)-A (*G*), VEGF receptor 1 (FLT-1; *H*), and VEGF receptor 2 (KDR; *I*). Data are means ± SE; $n = 4$ in the sham group, $n = 3$ in the microsphere infusion (Spheres) group, $n = 5$ in the N^{ω}-nitro-L-arginine methyl ester (L-NAME) group, and $n = 6$ in the L-NAME + Spheres group. No significant differences between groups were observed.

followup; *4*) impaired oxygenation of the arterial blood was compensated by a small increase in systemic oxygen extraction; and *5*) repeated embolizations initially resulted in RV dysfunction at rest, as assessed with echocardiography, and by a decrease in SVi during exercise. However, at the end of followup, the presence of RV hypertrophy was associated with a maintained SVi during exercise.

Induction of CTEPH requires both repeated embolizations and endothelial dysfunction. As shown in Table 1, over the past decades, several research groups have attempted to develop a large animal model of CTEPH using different embolization materials, particle sizes, and embolization frequencies. Many of these attempts have failed to show a sustained (>2 wk after the last embolization) increase in PAP (1, 21, 31, 37, 39, 42, 43, 51, 58, 63). The studies that did show a sustained increase in PAP (5, 20, 50, 53, 66) have in common that they embolized a large part of the pulmonary vasculature, with multiple embolization procedures. It has been suggested that 40–60% of the lung vasculature needs to be obstructed for CTEPH to develop (3, 14). Indeed, Boulate et al. (5) performed ligation of the left pulmonary artery in combination with progressive embolization of the segmental arteries of the right lower lobe, leaving the right upper and possibly right middle lobe unaffected.

Estimation of the relative magnitude of the obstructed part of the pulmonary vasculature requires comparison of the number of microspheres infused with the number of vascular branches of corresponding size present in the pulmonary vascular bed. The pulmonary vasculature can be morphometrically described with diameter-defined Strahler orders, starting at the capillaries and ending at the main pulmonary artery (28). The pulmonary vascular tree of swine is less well described than that of humans, in which a total of 15 orders were observed (28). In swine, pulmonary vascular morphometry of pulmonary arteries larger than 160 μm in diameter was analyzed using multidetector-row computed tomography, resulting in 10 branching orders (32). This number of branching orders corresponds well with the human study, in which vessels of the fifth order had an average diameter of 150 μm. In the present study, CTEPH was induced with embolizations using microspheres of 600–710 μm in diameter. This size of microspheres corresponds with order 3 (diameter 430 μm, range 380–570 μm) and order 4 (diameter: 760 μm, range: 660–990 μm), of which ~2,100 and 590 are present in the porcine pulmonary vasculature (32). It has to be taken into account that supernumerary vessels were not measured because of the computational model used. These supernumerary vessels are estimated to be present at ratios of 1.6 (47) or 2.8 (6) to conventional arteries. Adding these

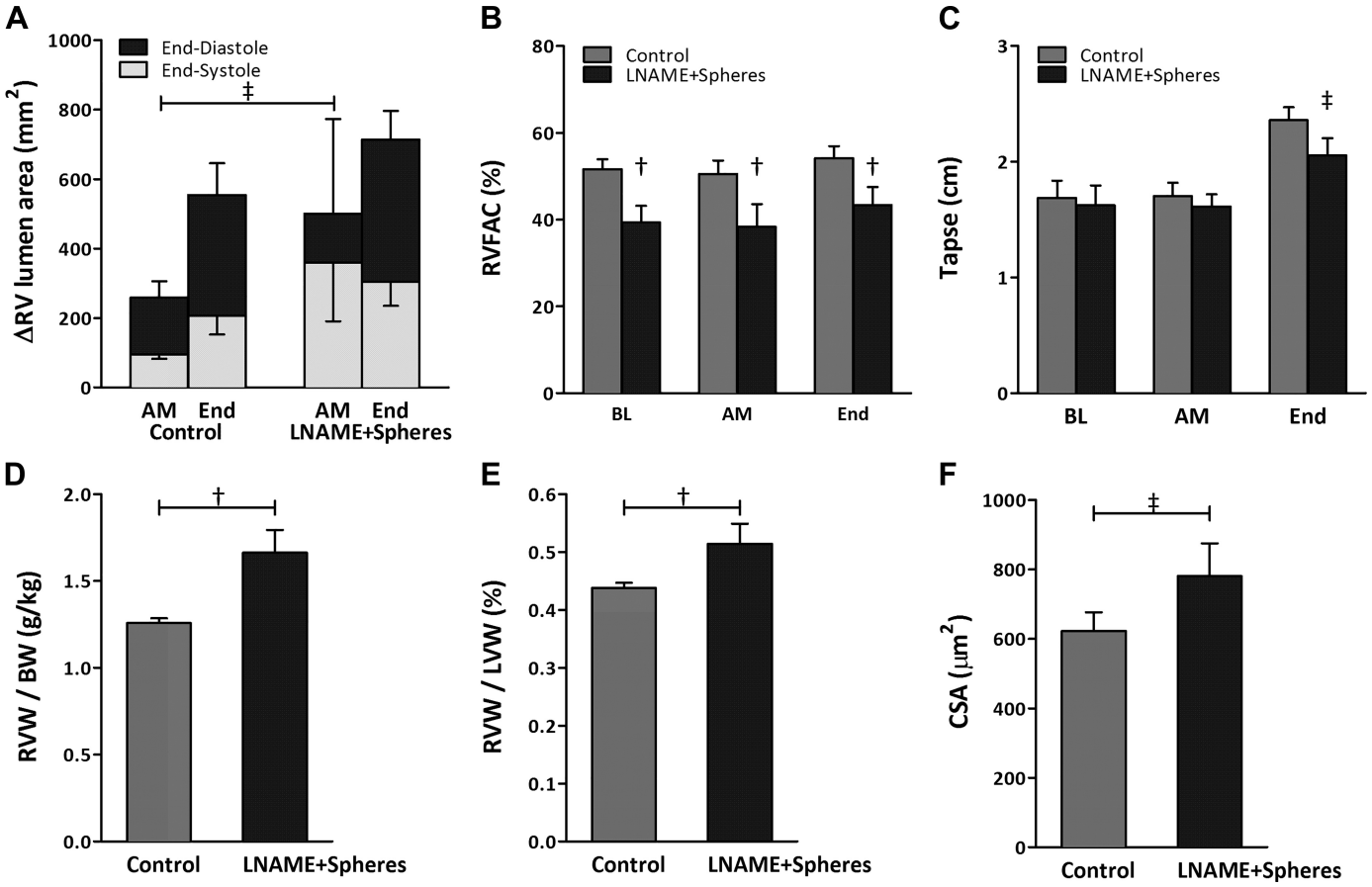

Fig. 6. Right ventricular (RV) remodeling. *A*: end-diastolic and end-systolic lumen area changes over time as measured with echocardiography versus baseline [*week 0*, before injection of N^{ω}-nitro-L-arginine methyl ester (L-NAME) and microsphere infusion (Spheres)]. End-systolic RV lumen area tended to be increased in the L-NAME + Spheres group compared with the control group at the end of the embolization period (AM) but not at the time point before euthanasia (End). *B*: RV fractional area change (RVFAC) was decreased at all time points in the L-NAME + Spheres vs. control group. *C*: tricuspid annular plane systolic excursion (TAPSE) tended to be increased in the L-NAME + Spheres group at the end time point versus the control group. *D*: RV weight (RVW) over body weight (BW) was increased at euthanasia. *E*: Fulton index [RVW over left ventricular weight (LVW)] was increased in the L-NAME + Spheres vs. control group. *F*: RV cardiomyocyte cross-sectional area (CSA) tended to be increased in the L-NAME + Spheres vs. control group at euthanasia. Data are means ± SE. *A*: control, AM $n = 6$ and End, $n = 9$; L-NAME + Spheres, AM $n = 5$ and End $n = 7$. *B* and *C*: control $n = 9$ and L-NAME + Spheres $n = 5$. *D–F*: control $n = 9$ and L-NAME+Spheres $n = 6$. ‡$P < 0.1$, L-NAME + Spheres vs. control at end systole; †$P < 0.05$, L-NAME + Spheres vs. control.

vessels to the number of vessels results in an estimated total of 5,460–7,980 arteries of order 3 and 1,530–2,240 arteries of order 4. Assuming that the pulmonary vascular tree of a 20-kg pig is threefold smaller than that of a 70-kg human, these numbers correspond well with the estimated 22,000 (order 8, diameter: 510 ± 40 μm) and 6,225 (order 9, diameter: 770 ± 70 μm) pulmonary small arteries present per lung in humans (28). To ensure full coverage of the pulmonary vasculature, microspheres were slowly injected into the RV, assuming that microspheres flow to perfused, nonembolized vessels. The presence of microspheres in all lung lobes was visually confirmed upon euthanization, and no microspheres were observed in systemic organs. Histologically, microspheres in the lungs were surrounded by fibrous tissue; however, quantitative PCR analyses revealed no changes in the expression of inflammatory markers IL-6, TNF-α, and TGF-β_1. Although some microspheres clustered, with an approximate total of 36,000 microspheres/animal, it is likely that 60% of these pulmonary small arteries were obstructed. Nevertheless, with microspheres alone, no sustained CTEPH developed.

Since CTEPH patients present with dysfunctional endothelium, as evidenced by alterations in coagulation, inflammation, angiogenesis, and vasoregulation (2, 35, 44, 55, 56), endothelial dysfunction was used as a second hit to induce CTEPH. Nitric oxide is an important endothelium-derived anticoagulatory, anti-inflammatory, proangiogenic vasodilator. Therefore, endothelial dysfunction was induced by inhibition of eNOS by chronic L-NAME administration, which, in combination with multiple microsphere infusions, resulted in a sustained increase in PAP and tPVRi. This increase in PAP above 25 mmHg for a prolonged period of time after embolizations and in the awake state is evidence for successful induction of chronic PH (1, 21, 31, 37, 39, 42, 43, 51, 53, 63, 66). Our findings are in accord with a recent study in rats that showed that sustained CTEPH developed when embolizations were combined with endothelial dysfunction produced by VEGF inhibition (41). Importantly, in the present study, CTEPH persisted when eNOS inhibition was discontinued, which, together with the reduced endothelium-dependent vasodilator response to substance P in isolated pulmonary small arteries, indicates that

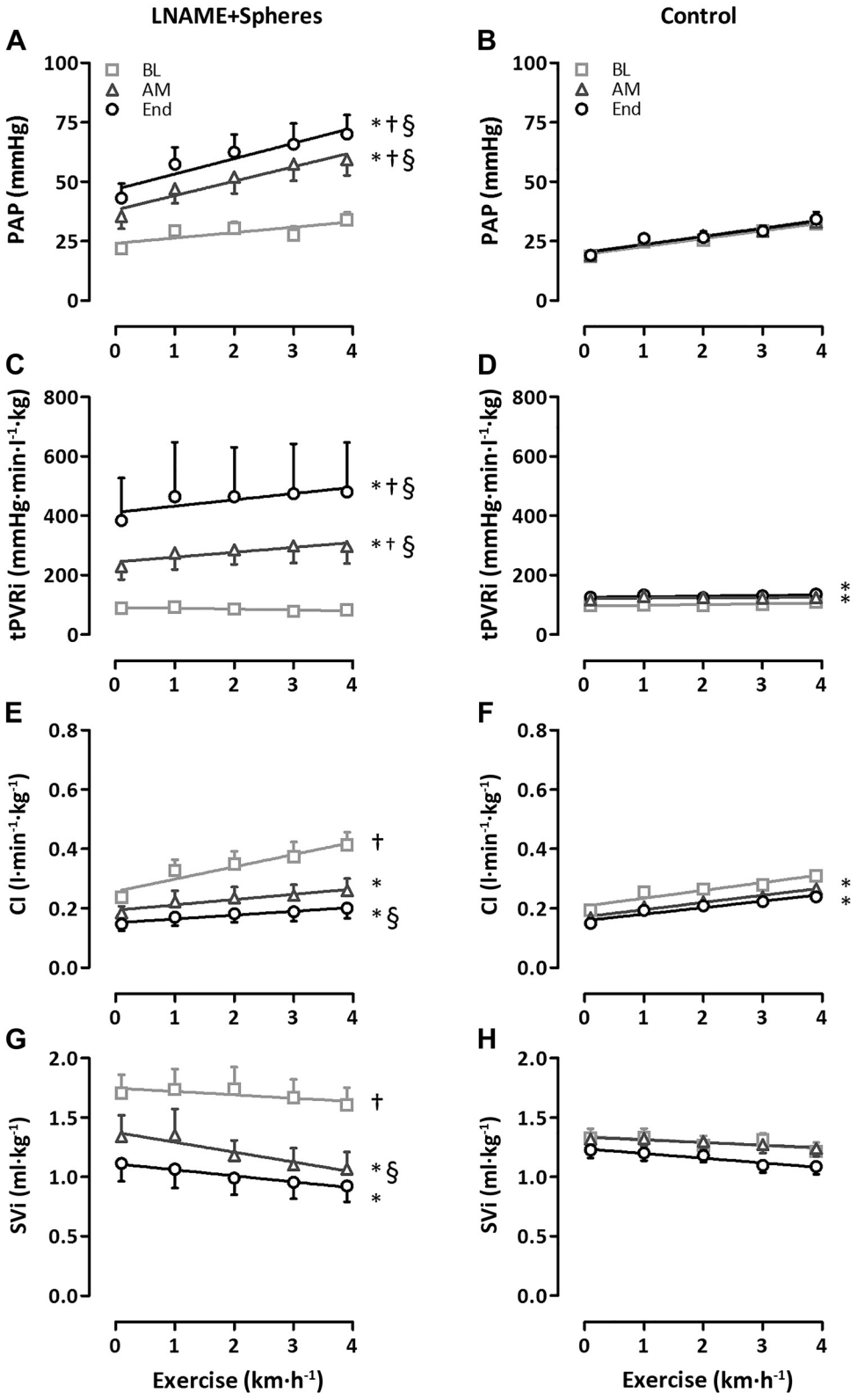

Fig. 7. Changes in pulmonary and cardiac hemodynamics during incremental levels of exercise at baseline (BL), after the completion of embolization (AM), and at the end of followup (End). Shown is the effect of exercise on mean pulmonary arterial pressure (PAP; *A* and *B*), total pulmonary vascular resistance index (tPVRi; *C* and *D*), cardiac index (CI; *E* and *F*), and stroke volume index (SVi; *G* and *H*). Data are means ± SE; $n = 12$ in the control group and $n = 6$ in the N^{ω}-nitro-L-arginine methyl ester + microsphere infused (L-NAME + Spheres) group. *$P < 0.05$ vs. BL; †$P < 0.05$ vs. the corresponding control value; §$P < 0.05$ vs. effect of exercise in the control group.

CTEPH in itself was sufficient to maintain a state of endothelial dysfunction. It is well established that, secondarily to pulmonary embolisms, worsening of PH results from progressive microvascular remodeling of the nonobstructed pulmonary small arteries (27, 38). Indeed, we also observed microvascular remodeling as evidenced by an increased wall thickness of the nonobstructed pulmonary small arteries and exaggerated vasoconstriction to both KCl and the thromboxane analog U-46619. Contrary to results in the lungs of patients with CTEPH, in which a reduction in VEGF expression and an elevation of the

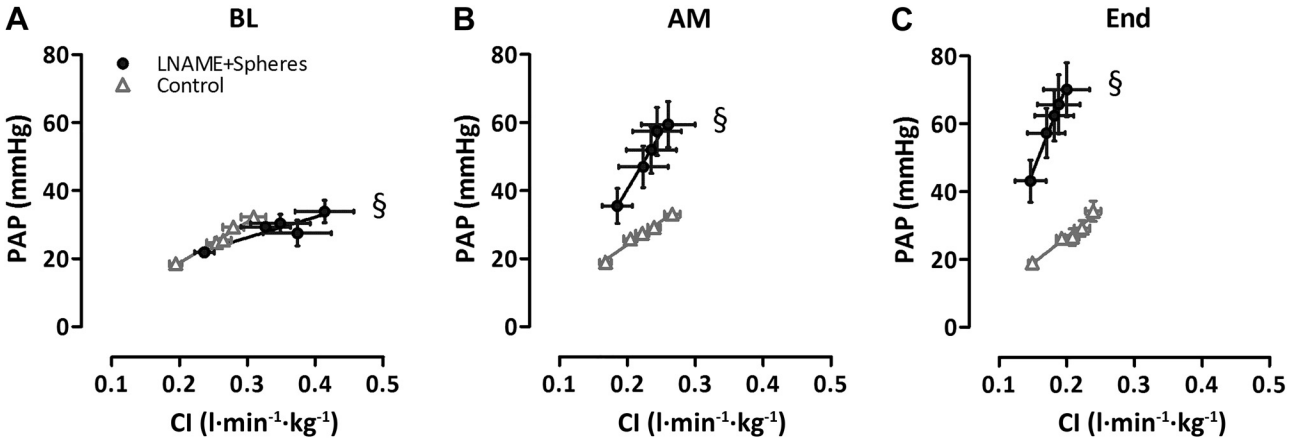

Fig. 8. Pulmonary vascular reserve. Shown is the relationship between pulmonary arterial pressure (PAP) and cardiac index (CI) during incremental exercise at baseline (BL; *A*), after the completion of embolization (AM; *B*), and at the end of followup (End; *C*). Data are means ± SE; $n = 12$ in the control group and $n = 6$ in the N^{ω}-nitro-L-arginine methyl ester + microsphere infused (L-NAME + Spheres) group. §$P < 0.05$, effect of exercise in the L-NAME + Spheres vs. control group (slope).

antiangiogenic factor angiopoietin-1 were observed (55), microvascular remodeling in our model was not accompanied by changes in expression of angiogenic factors as measured with quantitative PCR in tissues obtained at euthanization. The exact time course of microvascular remodeling cannot be determined from our data, as the increase in resistance due to embolization cannot be distinguished from the increase in resistance due to microvascular remodeling during the embolization period. However, tPVRi continued to increase after cessation of the embolization procedures, which is consistent with remodeling of the distal vasculature, although an increase in microvascular tone secondary to endothelial dysfunction may also have contributed.

Cardiopulmonary stress testing and RV function. Exercise testing after pulmonary embolism is predictive of development of PH and/or patient outcome in established CTEPH (22, 24, 25, 48). Swine were exercised on a motor-driven treadmill up to 4 km/h before induction of CTEPH and on a weekly basis during and after the embolization period to investigate the influence of cardiopulmonary stress on hemodynamic variables and blood oxygenation. Swine reached heart rates of ~255 beats/min at the beginning of the study and 210 beats/min at the final exercise trial (Table 3), whereas maximal heart rates of 272 beats/min have been reported in the literature in swine of similar size (64). Nevertheless, the significant lactate production during exercise at the beginning of the study as well as at the final exercise trial in the CTEPH swine suggests that near-maximal levels were reached at those time points.

In accord with Claessen and coworkers (7, 8), we observed that the RV was not able to cope with the increased afterload during exercise, as evidenced by decreased SVi, particularly early after embolization. Furthermore, whereas RV end-diastolic cross-sectional lumen area was unchanged, RV end-systolic cross-sectional lumen area tended to be increased, suggestive of systolic contractile dysfunction, although TAPSE was not different. The decreased SVi was not compensated by an increase in heart rate; hence, CI was lower in swine with CTEPH. Despite the blunted exercise-induced increase in CI, the increase in PAP and tPVRi were exacerbated during exercise. Moreover, the V/Q mismatch was exacerbated during exercise, resulting in a further decrease in arterial P_{O_2} during exercise.

At the end of followup, the time point that resembles the time when most patients present in the hospital with symptoms, PAP and tPVRi were still elevated at rest and, similarly to patients with CTEPH, the increase in PAP was exacerbated during exercise (7, 8). However, as a result of the chronically elevated RV afterload, the RV underwent hypertrophy as reflected by increases in RV weight/body weight, Fulton index, and cardiomyocyte cross-sectional area. Although TAPSE showed a trend toward a decrease in the L-NAME + Spheres group, RV hypertrophy blunted the systolic dysfunction of the heart, as observed using echocardiography at rest as well as the decrease in SVi during exercise. Nevertheless, CI was persistently decreased at rest and did not increase significantly during exercise. In addition, patients presenting with a V/Q mismatch in the lungs suffer a further decrease in ventilatory efficiency during exercise. Although this V/Q mismatch correlates to RV function in other types of PH, there is no correlation in either CTEPH patients or in L-NAME+Spheres animals in the present study (data not shown) (19, 46, 60). The reduction in oxygen uptake was exacerbated during exercise, as evidenced by a decrease in arterial P_{O_2}, which, in combination with the decreased CI, resulted in reduced maximal oxygen consumption (29, 36, 48). Similarly, in our swine model, the V/Q mismatch increased in severity with incremental exercise intensity, as evidenced by a further decrease in arterial P_{O_2}. This V/Q mismatch remained present during the entire followup period. However, given the relatively mild reduction in arterial P_{O_2}, the capability of the body to increase oxygen extraction, and the more severe reduction in SVi during exercise, it is likely that the main cause of the exercise limitations in CTEPH is cardiac insufficiency. These data in our porcine model are consistent with the observations by Claessen and coworkers (7, 8) that exercise intolerance in CTEPH patients is principally determined by a disproportional increase in RV afterload.

Conclusions. A combination of repeated embolization procedures and endothelial dysfunction was required to successfully develop a large-animal model for CTEPH. To the best of

Table 3. *Hemodynamics and blood gas values of swine at rest and during exercise at BL, AM, and at the end of followup*

	Rest	Exercise, km/h			
	0	1	2	3	4
		Heart rate, beats/min			
Control					
BL	149 ± 7	200 ± 10	219 ± 15	224 ± 11	255 ± 10
AM	128 ± 6	156 ± 6*	172 ± 6*	191 ± 7	219 ± 8*
End	128 ± 6*	153 ± 7*	169 ± 7*	195 ± 12	211 ± 12
L-NAME + Spheres					
BL	158 ± 7	191 ± 11	200 ± 10	221 ± 12	253 ± 9
AM	134 ± 8	162 ± 10	197 ± 14	218 ± 10	237 ± 10
End	129 ± 7*	157 ± 7*	175 ± 10	187 ± 15	209 ± 5*
		Mean arterial pressure, mmHg			
Control					
BL	88 ± 2	94 ± 2	92 ± 3	92 ± 3	92 ± 2
AM	90 ± 4	97 ± 3	101 ± 4*	102 ± 4	105 ± 4*
End	94 ± 4	98 ± 4	99 ± 4*	101 ± 5*	104 ± 5*
L-NAME + Spheres					
BL	88 ± 3	94 ± 2	90 ± 2	90 ± 3	92 ± 3
AM	103 ± 4*	109 ± 6	113 ± 6*	115 ± 5*	113 ± 5*
End	96 ± 7	104 ± 7	107 ± 9	107 ± 9	112 ± 10
		Systemic vascular resistance index, mmHg·min·l^{-1}·kg			
Control					
BL	463 ± 22	368 ± 17	357 ± 13	325 ± 14	320 ± 26
AM	550 ± 31*	485 ± 29*	456 ± 24*	425 ± 21*	395 ± 20*
End	624 ± 29*	552 ± 43*	517 ± 41*	497 ± 36*	482 ± 41*
L-NAME + Spheres					
BL	340 ± 29†	299 ± 25†	272 ± 24†	257 ± 24†	246 ± 14†
AM	590 ± 79*	494 ± 81	474 ± 72*	462 ± 65*	440 ± 68*
End	892 ± 283	917 ± 357	890 ± 340	562 ± 79*	554 ± 79*
		Left atrial pressure, mmHg			
Control					
BL	6 ± 1	8 ± 1	8 ± 1	9 ± 2	12 ± 2
AM	4 ± 1	7 ± 1	7 ± 1	7 ± 1	9 ± 1
End	8 ± 1	10 ± 1	10 ± 1	11 ± 1	12 ± 1
L-NAME + Spheres					
BL	10 ± 2†	12 ± 1†	11 ± 1	12 ± 1	12 ± 1
AM	8 ± 2	10 ± 1	10 ± 2	9 ± 2	15 ± 3†
End	9 ± 2	10 ± 3	10 ± 3	13 ± 3	17 ± 4
		Hemoglobin, g/dl			
Control					
BL	9.4 ± 0.3	10.0 ± 0.3	9.5 ± 0.3	10.0 ± 0.3	9.7 ± 0.3
AM	9.5 ± 0.3	9.8 ± 0.3	10.2 ± 0.3	10.1 ± 0.4	10.5 ± 0.4
End	10.0 ± 0.4	10.2 ± 0.4	10.8 ± 0.4*	10.9 ± 0.4*	11.1 ± 0.4*
L-NAME + Spheres					
BL	9.1 ± 0.4	9.2 ± 0.3	9.5 ± 0.3	9.3 ± 0.3	9.6 ± 0.3
AM	8.9 ± 0.3	9.2 ± 0.3	9.7 ± 0.4	10.0 ± 0.5	10.1 ± 0.6
End	9.2 ± 0.3	9.8 ± 0.2	9.8 ± 0.2*	10.3 ± 0.3*	10.6 ± 0.4
		Lactate, mmol/l			
Control					
BL	0.7 ± 0.1	0.9 ± 0.1	0.9 ± 0.2	1.2 ± 0.3	1.9 ± 0.3
AM	0.8 ± 0.1	0.7 ± 0.1	0.8 ± 0.1	0.9 ± 0.1	1.5 ± 0.2
End	0.7 ± 0.1	0.7 ± 0.1	0.7 ± 0.1	0.7 ± 0.1	1.4 ± 0.3
L-NAME + Spheres					
BL	0.9 ± 0.1	1.1 ± 0.1	1.0 ± 0.1	1.1 ± 0.2	1.8 ± 0.3
AM	0.9 ± 0.1	0.9 ± 0.1	1.2 ± 0.2	1.6 ± 0.2†	2.8 ± 0.5†
End	0.7 ± 0.1	0.9 ± 0.1	0.9 ± 0.1	1.2 ± 0.2	2.4 ± 1.0
		Arterial O_2 saturation, %			
Control					
BL	96 ± 1	94 ± 1	94 ± 1	94 ± 1	93 ± 1
AM	98 ± 1	97 ± 1	97 ± 1	97 ± 1	97 ± 1
End	97 ± 1	97 ± 1	96 ± 1	97 ± 1	96 ± 1
L-NAME + Spheres					
BL	97 ± 1	93 ± 1	94 ± 2	94 ± 2	93 ± 1
AM	95 ± 1†	91 ± 2†	89 ± 2†	91 ± 2†	91 ± 1†
End	96 ± 1	91 ± 2†	92 ± 3	92 ± 2	92 ± 2†

Data are presented as means ± SE; $n = 12$ animals in the control group and 6 animals in the N^{ω}-nitro-L-arginine methyl ester + microsphere infused (L-NAME + Spheres) group. BL, baseline; AM, after microsphere infusion; End, at the end of followup. *$P < 0.05$ vs. the corresponding BL value; †$P < 0.05$ vs. the corresponding value in the control group.

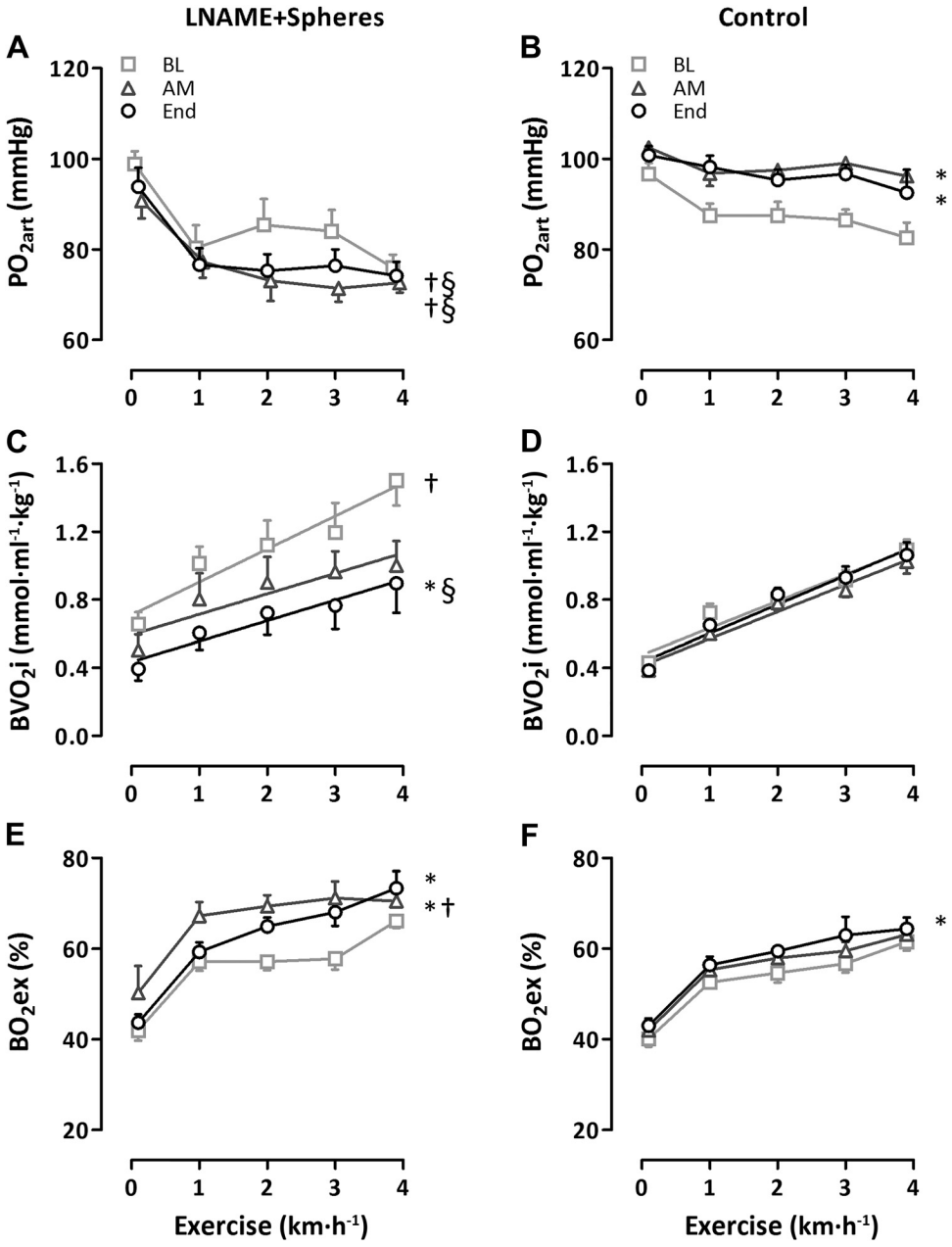

Fig. 9. Systemic oxygenation and body oxygen consumption during incremental levels of exercise at baseline (BL), after microspheres (AM), and at the end of followup (End). Shown is the effect of exercise on arterial P_{O_2} ($P_{O_{2art}}$; *A* and *B*), body oxygen consumption index ($B\dot{V}_{O_2}i$; *C* and *D*), and body oxygen extraction ($B\dot{V}_{O_2}ex$; *E* and *F*). Data are means ± SE; $n = 12$ in the control group and $n = 6$ in the N^{ω}-nitro-L-arginine methyl ester + microsphere infused (L-NAME + Spheres) group. $^*P < 0.05$ vs. BL; †$P < 0.05$ vs. the corresponding control value; §$P < 0.05$ vs. effect of exercise in the control group.

our knowledge, the present study is the first to investigate the role of both cardiac dysfunction and V/Q mismatch in exercise intolerance in an animal model of CTEPH. This model emulates critical features of patients with CTEPH, including V/Q mismatch and early RV dysfunction. The latter likely contributed to the reduced SVi that was present at rest. Both the V/Q mismatch and cardiac dysfunction were aggravated by exercise. Prolonged increases in RV afterload were associated with adaptive RV hypertrophy, while the V/Q mismatch remained present. This animal model can be further used to investigate disease development, early diagnostic markers, and interventions that interfere with microvascular remodeling in the field of CTEPH research. Finally, this model may also be used to delineate sex differences that are known to exist in development and progression of CTEPH (54).

ACKNOWLEDGMENTS

We acknowledge the technical support of Annemarie Verzijl, Ilona Krabbendam-Peters, Esther van de Kamp, Dylan van der Vusse, Brechje de Rapper, and Paula Krul.

GRANTS

This work was supported by the Netherlands CardioVascular Research Initiative, the Dutch Heart Foundation, the Dutch Federation of University Medical Centers, The Netherlands Organization for Health Research and Development, and the Royal Netherlands Academy of Science (CVON2012-08, Phaedra).

DISCLOSURES

No conflicts of interest, financial or otherwise, are declared by the authors.

AUTHOR CONTRIBUTIONS

K.S., D.J.D., and D.M. conceived and designed research; K.S., R.W.B.v.D., and Z.C. performed experiments; K.S. and Z.C. analyzed data; K.S., R.W-.B.v.D., A.U., Z.C., D.J.D., and D.M. interpreted results of experiments; K.S. prepared figures; K.S. drafted manuscript; K.S., R.W.B.v.D., A.U., D.J.D., and D.M. edited and revised manuscript; K.S., R.W.B.v.D., A.U., Z.C., D.J.D., and D.M. approved final version of manuscript.

REFERENCES

1. **Aguero J, Ishikawa K, Fish KM, Hammoudi N, Hadri L, Garcia-Alvarez A, Ibanez B, Fuster V, Hajjar RJ, Leopold JA.** Combination proximal pulmonary artery coiling and distal embolization induces chronic elevations in pulmonary artery pressure in Swine. *PLoS One* 10: e0124526, 2015. doi:10.1371/journal.pone.0124526.
2. **Alias S, Redwan B, Panzenboeck A, Winter MP, Schubert U, Voswinckel R, Frey MK, Jakowitsch J, Alimohammadi A, Hobohm L, Mangold A, Bergmeister H, Sibilia M, Wagner EF, Mayer E, Klepetko W, Hoelzenbein TJ, Preissner KT, Lang IM.** Defective angiogenesis delays thrombus resolution: a potential pathogenetic mechanism underlying chronic thromboembolic pulmonary hypertension. *Arterioscler Thromb Vasc Biol* 34: 810–819, 2014. doi:10.1161/ATVBAHA.113.302991.
3. **Azarian R, Wartski M, Collignon MA, Parent F, Hervé P, Sors H, Simonneau G.** Lung perfusion scans and hemodynamics in acute and chronic pulmonary embolism. *J Nucl Med* 38: 980–983, 1997.
4. **Beam DM, Neto-Neves EM, Stubblefield WB, Alves NJ, Tune JD, Kline JA.** Comparison of isoflurane and α-chloralose in an anesthetized swine model of acute pulmonary embolism producing right ventricular dysfunction. *Comp Med* 65: 54–61, 2015.
5. **Boulate D, Perros F, Dorfmuller P, Arthur-Ataam J, Guihaire J, Lamrani L, Decante B, Humbert M, Eddahibi S, Dartevelle P, Fadel E, Mercier O.** Pulmonary microvascular lesions regress in reperfused chronic thromboembolic pulmonary hypertension. *J Heart Lung Transplant* 34: 457–467, 2015. doi:10.1016/j.healun.2014.07.005.
6. **Burrowes KS, Hunter PJ, Tawhai MH.** Anatomically based finite element models of the human pulmonary arterial and venous trees including supernumerary vessels. *J Appl Physiol* 99: 731–738, 2005. doi:10.1152/japplphysiol.01033.2004.
7. **Claessen G, La Gerche A, Dymarkowski S, Claus P, Delcroix M, Heidbuchel H.** Pulmonary vascular and right ventricular reserve in patients with normalized resting hemodynamics after pulmonary endarterectomy. *J Am Heart Assoc* 4: e001602, 2015. doi:10.1161/JAHA.114.001602.
8. **Claessen G, La Gerche A, Wielandts JY, Bogaert J, Van Cleemput J, Wuyts W, Claus P, Delcroix M, Heidbuchel H.** Exercise pathophysiology and sildenafil effects in chronic thromboembolic pulmonary hypertension. *Heart* 101: 637–644, 2015. doi:10.1136/heartjnl-2014-306851.
9. **Claeys MA, Gepts E, Camu F.** Haemodynamic changes during anaesthesia induced and maintained with propofol. *Br J Anaesth* 60: 3–9, 1988. doi:10.1093/bja/60.1.3.
10. **De Wijs-Meijler DP, Stam K, van Duin RW, Verzijl A, Reiss IK, Duncker DJ, Merkus D.** Surgical placement of catheters for long-term cardiovascular exercise testing in swine. *J Vis Exp* 2016: e53772, 2016.
11. **de Wijs-Meijler DPM, Danser AHJ, Reiss IKM, Duncker DJ, Merkus D.** Sex differences in pulmonary vascular control: focus on the nitric oxide pathway. *Physiol Rep* 5: 5, 2017. doi:10.14814/phy2.13200.
12. **Duncker DJ, Stubenitsky R, Verdouw PD.** Role of adenosine in the regulation of coronary blood flow in swine at rest and during treadmill exercise. *Am J Physiol Heart Circ Physiol* 275: H1663–H1672, 1998.
13. **Edward JA, Mandras S.** An update on the management of chronic thromboembolic pulmonary hypertension. *Curr Probl Cardiol* 42: 7–38, 2017. doi:10.1016/j.cpcardiol.2016.11.001.
14. **Fedullo PF, Auger WR, Kerr KM, Rubin LJ.** Chronic thromboembolic pulmonary hypertension. *N Engl J Med* 345: 1465–1472, 2001. doi:10.1056/NEJMra010902.
15. **Galiè N, Humbert M, Vachiery JL, Gibbs S, Lang I, Torbicki A, Simonneau G, Peacock A, Vonk Noordegraaf A, Beghetti M, Ghofrani A, Gomez Sanchez MA, Hansmann G, Klepetko W, Lancellotti P, Matucci M, McDonagh T, Pierard LA, Trindade PT, Zompatori M, Hoeper M.** 2015 ESC/ERS Guidelines for the diagnosis and treatment of pulmonary hypertension: the Joint Task Force for the Diagnosis and Treatment of Pulmonary Hypertension of the European Society of Cardiology (ESC) and the European Respiratory Society (ERS): endorsed by: Association for European Paediatric and Congenital Cardiology (AEPC), International Society for Heart and Lung Transplantation (ISHLT). *Eur Respir J* 46: 903–975, 2015. doi:10.1183/13993003.01032-2015.
16. **Galiè N, Kim NH.** Pulmonary microvascular disease in chronic thromboembolic pulmonary hypertension. *Proc Am Thorac Soc* 3: 571–576, 2006. doi:10.1513/pats.200605-113LR.
17. **Gall H, Preston IR, Hinzmann B, Heinz S, Jenkins D, Kim NH, Lang I.** An international physician survey of chronic thromboembolic pulmonary hypertension management. *Pulm Circ* 6: 472–482, 2016. doi:10.1086/688084.
18. **García-Álvarez A, Fernández-Friera L, García-Ruiz JM, Nuño-Ayala M, Pereda D, Fernández-Jiménez R, Guzmán G, Sanchez-Quintana D, Alberich-Bayarri A, Pastor-Escuredo D, Sanz-Rosa D, García-Prieto J, Gonzalez-Mirelis JG, Pizarro G, Jimenez-Borreguero LJ, Fuster V, Sanz J, Ibáñez B.** Noninvasive monitoring of serial changes in pulmonary vascular resistance and acute vasodilator testing using cardiac magnetic resonance. *J Am Coll Cardiol* 62: 1621–1631, 2013. doi:10.1016/j.jacc.2013.07.037.
19. **Gopalan D, Delcroix M, Held M.** Diagnosis of chronic thromboembolic pulmonary hypertension. *Eur Respir Rev* 26: 160108, 2017. doi:10.1183/16000617.0108-2016.
20. **Guihaire J, Haddad F, Boulate D, Capderou A, Decante B, Flécher E, Eddahibi S, Dorfmüller P, Hervé P, Humbert M, Verhoye JP, Dartevelle P, Mercier O, Fadel E.** Right ventricular plasticity in a porcine model of chronic pressure overload. *J Heart Lung Transplant* 33: 194–202, 2014. doi:10.1016/j.healun.2013.10.026.
21. **Guihaire J, Haddad F, Noly PE, Boulate D, Decante B, Dartevelle P, Humbert M, Verhoye JP, Mercier O, Fadel E.** Right ventricular reserve in a piglet model of chronic pulmonary hypertension. *Eur Respir J* 45: 709–717, 2015. doi:10.1183/09031936.00081314.
22. **Hasler ED, Müller-Mottet S, Furian M, Saxer S, Huber LC, Maggiorini M, Speich R, Bloch KE, Ulrich S.** Pressure-flow during exercise catheterization predicts survival in pulmonary hypertension. *Chest* 150: 57–67, 2016. doi:10.1016/j.chest.2016.02.634.
23. **Haythe J.** Chronic thromboembolic pulmonary hypertension: a review of current practice. *Prog Cardiovasc Dis* 55: 134–143, 2012. doi:10.1016/j.pcad.2012.07.005.
24. **Held M, Grün M, Holl R, Hübner G, Kaiser R, Karl S, Kolb M, Schäfers HJ, Wilkens H, Jany B.** Cardiopulmonary exercise testing to detect chronic thromboembolic pulmonary hypertension in patients with normal echocardiography. *Respiration* 87: 379–387, 2014. doi:10.1159/000358565.
25. **Held M, Hesse A, Gött F, Holl R, Hübner G, Kolb P, Langen HJ, Romen T, Walter F, Schäfers HJ, Wilkens H, Jany B.** A symptom-related monitoring program following pulmonary embolism for the early detection of CTEPH: a prospective observational registry study. *BMC Pulm Med* 14: 141, 2014. doi:10.1186/1471-2466-14-141.
26. **Hoeper MM, Bogaard HJ, Condliffe R, Frantz R, Khanna D, Kurzyna M, Langleben D, Manes A, Satoh T, Torres F, Wilkins MR, Badesch DB.** Definitions and diagnosis of pulmonary hypertension. *J Am Coll Cardiol* 62, *Suppl*: D42–D50, 2013. doi:10.1016/j.jacc.2013.10.032.
27. **Hoeper MM, Mayer E, Simonneau G, Rubin LJ.** Chronic thromboembolic pulmonary hypertension. *Circulation* 113: 2011–2020, 2006. doi:10.1161/CIRCULATIONAHA.105.602565.
28. **Huang W, Yen RT, McLaurine M, Bledsoe G.** Morphometry of the human pulmonary vasculature. *J Appl Physiol* 81: 2123–2133, 1996. doi:10.1152/jappl.1996.81.5.2123.
29. **Iwase T, Nagaya N, Ando M, Satoh T, Sakamaki F, Kyotani S, Takaki H, Goto Y, Ohkita Y, Uematsu M, Nakanishi N, Miyatake K.** Acute and chronic effects of surgical thromboendarterectomy on exercise capacity and ventilatory efficiency in patients with chronic thromboembolic pulmonary hypertension. *Heart* 86: 188–192, 2001. doi:10.1136/heart.86.2.188.
30. **Jamieson SW, Kapelanski DP, Sakakibara N, Manecke GR, Thistlethwaite PA, Kerr KM, Channick RN, Fedullo PF, Auger WR.** Pulmonary endarterectomy: experience and lessons learned in 1,500 cases. *Ann Thorac Surg* 76: 1457–1462; discussion 1462–1454, 2003.
31. **Kim H, Yung GL, Marsh JJ, Konopka RG, Pedersen CA, Chiles PG, Morris TA, Channick RN.** Endothelin mediates pulmonary vascular remodelling in a canine model of chronic embolic pulmonary hypertension. *Eur Respir J* 15: 640–648, 2000. doi:10.1034/j.1399-3003.2000.15d04.x.
32. **Lee YC, Clark AR, Fuld MK, Haynes S, Divekar AA, Hoffman EA, Tawhai MH.** MDCT-based quantification of porcine pulmonary arterial

morphometry and self-similarity of arterial branching geometry. *J Appl Physiol* 114: 1191–1201, 2013. doi:10.1152/japplphysiol.00868.2012.
33. **Lin YJ, Markham NE, Balasubramaniam V, Tang JR, Maxey A, Kinsella JP, Abman SH.** Inhaled nitric oxide enhances distal lung growth after exposure to hyperoxia in neonatal rats. *Pediatr Res* 58: 22–29, 2005. doi:10.1203/01.PDR.0000163378.94837.3E.
34. **Matsunaga T, Warltier DC, Weihrauch DW, Moniz M, Tessmer J, Chilian WM.** Ischemia-induced coronary collateral growth is dependent on vascular endothelial growth factor and nitric oxide. *Circulation* 102: 3098–3103, 2000. doi:10.1161/01.CIR.102.25.3098.
35. **Matthews DT, Hemnes AR.** Current concepts in the pathogenesis of chronic thromboembolic pulmonary hypertension. *Pulm Circ* 6: 145–154, 2016. doi:10.1086/686011.
36. **McCabe C, Deboeck G, Harvey I, Ross RM, Gopalan D, Screaton N, Pepke-Zaba J.** Inefficient exercise gas exchange identifies pulmonary hypertension in chronic thromboembolic obstruction following pulmonary embolism. *Thromb Res* 132: 659–665, 2013. doi:10.1016/j.thromres.2013.09.032.
37. **Mercier O, Tivane A, Dorfmüller P, de Perrot M, Raoux F, Decante B, Eddahibi S, Dartevelle P, Fadel E.** Piglet model of chronic pulmonary hypertension. *Pulm Circ* 3: 908–915, 2013. doi:10.1086/674757.
38. **Moser KM, Bloor CM.** Pulmonary vascular lesions occurring in patients with chronic major vessel thromboembolic pulmonary hypertension. *Chest* 103: 685–692, 1993. doi:10.1378/chest.103.3.685.
39. **Moser KM, Cantor JP, Olman M, Villespin I, Graif JL, Konopka R, Marsh JJ, Pedersen C.** Chronic pulmonary thromboembolism in dogs treated with tranexamic acid. *Circulation* 83: 1371–1379, 1991. doi:10.1161/01.CIR.83.4.1371.
40. **Mulvany MJ, Halpern W.** Contractile properties of small arterial resistance vessels in spontaneously hypertensive and normotensive rats. *Circ Res* 41: 19–26, 1977. doi:10.1161/01.RES.41.1.19.
41. **Neto-Neves EM, Brown MB, Zaretskaia MV, Rezania S, Goodwill AG, McCarthy BP, Persohn SA, Territo PR, Kline JA.** Chronic embolic pulmonary hypertension caused by pulmonary embolism and vascular endothelial growth factor inhibition. *Am J Pathol* 187: 700–712, 2017. doi:10.1016/j.ajpath.2016.12.004.
42. **Perkett EA, Brigham KL, Meyrick B.** Continuous air embolization into sheep causes sustained pulmonary hypertension and increased pulmonary vasoreactivity. *Am J Pathol* 132: 444–454, 1988.
43. **Pohlmann JR, Akay B, Camboni D, Koch KL, Mervak BM, Cook KE.** A low mortality model of chronic pulmonary hypertension in sheep. *J Surg Res* 175: 44–48, 2012. doi:10.1016/j.jss.2011.02.049.
44. **Quarck R, Wynants M, Ronisz A, Sepulveda MR, Wuytack F, Van Raemdonck D, Meyns B, Delcroix M.** Characterization of proximal pulmonary arterial cells from chronic thromboembolic pulmonary hypertension patients. *Respir Res* 13: 27, 2012. doi:10.1186/1465-9921-13-27.
45. **Rees DD, Palmer RM, Schulz R, Hodson HF, Moncada S.** Characterization of three inhibitors of endothelial nitric oxide synthase in vitro and in vivo. *Br J Pharmacol* 101: 746–752, 1990. doi:10.1111/j.1476-5381.1990.tb14151.x.
46. **Rehman MB, Howard LS, Christiaens LP, Gill D, Gibbs JS, Nihoyannopoulos P.** Resting right ventricular function is associated with exercise performance in PAH, but not in CTEPH. *Eur Heart J Cardiovasc Imaging*. In press. doi:10.1093/ehjci/jex002.
47. **Rendas A, Branthwaite M, Reid L.** Growth of pulmonary circulation in normal pig–structural analysis and cardiopulmonary function. *J Appl Physiol Respir Environ Exerc Physiol* 45: 806–817, 1978.
48. **Richter MJ, Pader P, Gall H, Reichenberger F, Seeger W, Mayer E, Guth S, Kramm T, Grimminger F, Ghofrani HA, Voswinckel R.** The prognostic relevance of oxygen uptake in inoperable chronic thromboembolic pulmonary hypertension. *Clin Respir J* 11: 682−690, 2017. doi:10.1111/crj.12399.
49. **Roehl AB, Steendijk P, Rossaint R, Bleilevens C, Goetzenich A, Hein M.** Xenon is not superior to isoflurane on cardiovascular function during experimental acute pulmonary hypertension. *Acta Anaesthesiol Scand* 56: 449–458, 2012. doi:10.1111/j.1399-6576.2011.02624.x.
50. **Rothman A, Wiencek RG, Davidson S, Evans WN, Restrepo H, Sarukhanov V, Mann D.** Challenges in the development of chronic pulmonary hypertension models in large animals. *Pulm Circ* 7: 156–166, 2017. doi:10.1086/690099.
51. **Sage E, Mercier O, Herve P, Tu L, Dartevelle P, Eddahibi S, Fadel E.** Right lung ischemia induces contralateral pulmonary vasculopathy in an animal model. *J Thorac Cardiovasc Surg* 143: 967–973, 2012. doi:10.1016/j.jtcvs.2011.12.052.
52. **Sharma T, Lau EM, Choudhary P, Torzillo PJ, Munoz PA, Simmons LR, Naeije R, Celermajer DS.** Dobutamine stress for evaluation of right ventricular reserve in pulmonary arterial hypertension. *Eur Respir J* 45: 700–708, 2015. doi:10.1183/09031936.00089914.
53. **Shelub I, van Grondelle A, McCullough R, Hofmeister S, Reeves JT.** A model of embolic chronic pulmonary hypertension in the dog. *J Appl Physiol Respir Environ Exerc Physiol* 56: 810–815, 1984.
54. **Shigeta A, Tanabe N, Shimizu H, Hoshino S, Maruoka M, Sakao S, Tada Y, Kasahara Y, Takiguchi Y, Tatsumi K, Masuda M, Kuriyama T.** Gender differences in chronic thromboembolic pulmonary hypertension in Japan. *Circ J* 72: 2069–2074, 2008. doi:10.1253/circj.CJ-08-0377.
55. **Simonneau G, Torbicki A, Dorfmüller P, Kim N.** The pathophysiology of chronic thromboembolic pulmonary hypertension. *Eur Respir Rev* 26: 160112, 2017. doi:10.1183/16000617.0112-2016.
56. **Skoro-Sajer N, Mittermayer F, Panzenboeck A, Bonderman D, Sadushi R, Hitsch R, Jakowitsch J, Klepetko W, Kneussl MP, Wolzt M, Lang IM.** Asymmetric dimethylarginine is increased in chronic thromboembolic pulmonary hypertension. *Am J Respir Crit Care Med* 176: 1154–1160, 2007. doi:10.1164/rccm.200702-278OC.
57. **Stubenitsky R, Verdouw PD, Duncker DJ.** Autonomic control of cardiovascular performance and whole body O2 delivery and utilization in swine during treadmill exercise. *Cardiovasc Res* 39: 459–474, 1998. doi:10.1016/S0008-6363(98)00102-3.
58. **Tang CX, Yang GF, Schoepf UJ, Han ZH, Qi L, Zhao YE, Wu J, Zhou CS, Zhu H, Stubenrauch AC, Mangold S, Zhang LJ, Lu GM.** Chronic thromboembolic pulmonary hypertension: comparison of dual-energy computed tomography and single photon emission computed tomography in canines. *Eur J Radiol* 85: 498–506, 2016. doi:10.1016/j.ejrad.2015.11.035.
59. **Torbicki A.** Hypertension: definition of pulmonary hypertension challenged? *Nat Rev Cardiol* 13: 250–251, 2016. doi:10.1038/nrcardio.2016.44.
60. **Tsuboi Y, Tanaka H, Nishio R, Sawa T, Terashita D, Nakayama K, Satomi-Kobayashi S, Sakai Y, Emoto N, Hirata KI.** Associations of exercise tolerance with hemodynamic parameters for pulmonary arterial hypertension and for chronic thromboembolic pulmonary hypertension. *J Cardiopulm Rehabil Prev* 37: 341–346, 2017. doi:10.1097/HCR.0000000000000257.
61. **Vavera Z, Vojacek J, Pudil R, Maly J, Elias P.** Chronic thromboembolic pulmonary hypertension after the first episode of pulmonary embolism? How often? *Biomed Pap Med Fac Univ Palacky Olomouc Czech Repub* 160: 125–129, 2016.
62. **Víteček J, Lojek A, Valacchi G, Kubala L.** Arginine-based inhibitors of nitric oxide synthase: therapeutic potential and challenges. *Mediators Inflamm* 2012: 318087, 2012. doi:10.1155/2012/318087.
63. **Weimann J, Zink W, Schnabel PA, Jakob H, Gebhard MM, Martin E, Motsch J.** Selective vasodilation by nitric oxide inhalation during sustained pulmonary hypertension following recurrent microembolism in pigs. *J Crit Care* 14: 133–140, 1999. doi:10.1016/S0883-9441(99)90026-6.
64. **White FC, McKirnan MD, Breisch EA, Guth BD, Liu YM, Bloor CM.** Adaptation of the left ventricle to exercise-induced hypertrophy. *J Appl Physiol* 62: 1097–1110, 1987. doi:10.1152/jappl.1987.62.3.1097.
65. **Yang S, Yang Y, Zhai Z, Kuang T, Gong J, Zhang S, Zhu J, Liang L, Shen YH, Wang C.** Incidence and risk factors of chronic thromboembolic pulmonary hypertension in patients after acute pulmonary embolism. *J Thorac Dis* 7: 1927–1938, 2015.
66. **Zhou X, Wang D, Castro CY, Hawkins H, Lynch JE, Liu X, Zwischenberger JB.** A pulmonary hypertension model induced by continuous pulmonary air embolization. *J Surg Res* 170: e11–e16, 2011. doi:10.1016/j.jss.2011.04.030.